Meteoritics & Planetary Science 36, 1189–1216 (2001)
Available online at http://www.uark.edu/meteor

Refractory calcium-aluminum-rich inclusions and aluminum-diopside-rich chondrules in the metal-rich chondrites Hammadah al Hamra 237 and Queen Alexandra Range 94411

ALEXANDER N. KROT[1]*, KEVIN D. MCKEEGAN[2], SARA S. RUSSELL[3], ANDERS MEIBOM[4], MICHAEL K. WEISBERG[5], JUTTA ZIPFEL[6], TATIANA V. KROT[1], TIMOTHY J. FAGAN[1] AND KLAUS KEIL[1]

[1]Hawaii Institute of Geophysics and Planetology, School of Ocean and Earth Science and Technology, University of Hawaii at Manoa, Honolulu, Hawaii 96822, USA
[2]Department of Earth and Space Sciences, University of California, Los Angeles, California 90095-1567, USA
[3]Department of Mineralogy, The Natural History Museum, Cromwell Road, London, SW7 5BD, U.K.
[4]Stanford University, Geological and Environmental Sciences, Stanford, California 94305-2115, USA
[5]Department of Physical Sciences, Kingsborough College, 2001 Oriental Boulevard, Brooklyn, New York 11235, USA
[6]Max-Planck-Institut für Chemie Abteilung Kosmochemie, P.O. Box 3060, D-55020 Mainz, Germany
*Correspondence author's e-mail address: sasha@pgd.hawaii.edu

(Received 2000 December 15; accepted in revised form 2001 May 24)

Abstract–The metal-rich chondrites Hammadah al Hamra (HH) 237 and Queen Alexandra Range (QUE) 94411, paired with QUE 94627, contain relatively rare (<1 vol%) calcium-aluminum-rich inclusions (CAIs) and Al-diopside-rich chondrules. Forty CAIs and CAI fragments and seven Al-diopside-rich chondrules were identified in HH 237 and QUE 94411/94627. The CAIs, ~50–400 μm in apparent diameter, include (a) 22 (56%) pyroxene-spinel ± melilite (+forsterite rim), (b) 11 (28%) forsterite-bearing, pyroxene-spinel ± melilite ± anorthite (+forsterite rim) (c) 2 (5%) grossite-rich (+spinel-melilite-pyroxene rim), (d) 2 (5%) hibonite-melilite (+spinel-pyroxene ± forsterite rim), (e) 1 (2%) hibonite-bearing, spinel-perovskite (+melilite-pyroxene rim), (f) 1 (2%) spinel-melilite-pyroxene-anorthite, and (g) 1 (2%) amoeboid olivine aggregate. Each type of CAI is known to exist in other chondrite groups, but the high abundance of pyroxene-spinel ± melilite CAIs with igneous textures and surrounded by a forsterite rim are unique features of HH 237 and QUE 94411/94627. Additionally, oxygen isotopes consistently show relatively heavy compositions with $\Delta^{17}O$ ranging from –6‰ to –10‰ ($1\sigma = 1.3$‰) for all analyzed CAI minerals (grossite, hibonite, melilite, pyroxene, spinel). This suggests that the CAIs formed in a reservoir isotopically distinct from the reservoir(s) where "normal", ^{16}O-rich ($\Delta^{17}O < -20$‰) CAIs in most other chondritic meteorites formed.

The Al-diopside-rich chondrules, which have previously been observed in CH chondrites and the unique carbonaceous chondrite Adelaide, contain Al-diopside grains enclosing oriented inclusions of forsterite, and interstitial anorthitic mesostasis and Al-rich, Ca-poor pyroxene, occasionally enclosing spinel and forsterite. These chondrules are mineralogically similar to the Al-rich barred-olivine chondrules in HH 237 and QUE 94411/94627, but have lower Cr concentrations than the latter, indicating that they may have formed during the same chondrule-forming event, but at slightly different ambient nebular temperatures. Aluminum-diopside grains from two Al-diopside-rich chondrules have O-isotopic compositions ($\Delta^{17}O \approx -7 \pm 1.1$‰) similar to CAI minerals, suggesting that they formed from an isotopically similar reservoir. The oxygen-isotopic composition of one Ca, Al-poor cryptocrystalline chondrule in QUE 94411/94627 was analyzed and found to have $\Delta^{17}O \approx -3 \pm 1.4$‰.

The characteristics of the CAIs in HH 237 and QUE 94411/94627 are inconsistent with an impact origin of these metal-rich meteorites. Instead they suggest that the components in CB chondrites are pristine products of large-scale, high-temperature processes in the solar nebula and should be considered *bona fide* chondrites.

Prelude preprint MS#4480

TABLE 1. List of CAIs and Al-diopside-rich chondrules studied in Hammadah al Hamra 237 and QUE 94411/94627.

Chondrite	ps	CAI no.	Core mineralogy								Rim mineralogy			
			hb	grs	pv	mel	sp	cpx	fo	an	mel	sp	cpx	fo
Hibonite-rich/bearing CAIs														
HH 237	l	#4-1	+	–	+	+	+	–	–	–	–	+	+	+
HH 237	AM	#4	+	–	–	+	+	–	–	–	+	–	+	–
HH 237	ls	#11	+	–	+	–	+	–	–	–	+	–	+	–
Grossite-rich CAIs														
HH 237	s	#1	–	+	–	–	–	–	–	–	+	+	+	–
QUE 94411	4	#3, fr	–	+	–	–	–	–	–	–	–	–	–	–
Pyroxene-spinel ± melilite CAIs and fragments														
HH 237	AM	#1	–	–	–	+	+	+	–	–	–	–	–	+
QUE 94411	4	#2, fr	–	–	–	+	–	–	–	–	–	–	–	–
QUE 94627	4	#A	–	–	–	+	+	+	–	–	–	–	–	+
QUE 94627	4	#C	–	–	+	–	+	–	–	+	+	–	+	–
HH 237	ss	#1	–	–	+	+	+	+	–	–	–	–	–	+
HH 237	ss	#2	–	–	+	+	+	+	–	–	+	–	+	–
HH 237	ls	#7	–	–	–	+	+	+	–	–	–	–	–	+
HH 237	ls	#9	–	–	–	+	+	+	–	–	–	–	–	+
HH 237	ls	#9a	–	–	–	+	–	–	–	–	–	+	+	+
HH 237	ls	#14	–	–	+	+	+	+	–	–	–	–	–	+
HH 237	ls	#15, fr	–	–	–	+	+	–	–	–	–	–	–	–
HH 237	l	#1-2	–	–	–	–	+	+	–	–	–	–	–	+
HH 237	l	#3-1	–	–	–	–	+	+	–	–	–	–	–	+
HH 237	l	#4-2	–	–	–	+	+	+	–	–	–	–	–	+
HH 237	AM	#6, fr	–	–	–	–	+	–	–	–	–	–	–	–
QUE 94411	4	#1	–	–	–	–	+	+	–	–	–	–	–	+
QUE 94411	4	#5, fr	–	–	–	–	+	+	–	–	–	–	–	–
HH 237	s	#3	–	–	–	–	+	+	–	–	–	–	–	+
HH 237	AM	#5, fr	–	–	–	–	–	+	–	–	–	–	–	–
QUE 94411	6	#1	–	–	–	–	–	+	–	–	–	–	–	+
QUE 94627	4	#D, fr	–	–	–	–	–	+	–	–	–	–	–	–
HH 237	ls	#5	–	–	–	–	–	+	–	–	–	–	–	+
HH 237	ls	#12	–	–	–	–	–	+	–	–	–	–	–	+
HH 237	s	#2, fr	–	–	–	–	–	+	–	–	–	–	–	–
Forsterite-bearing, pyroxene-spinel ± melilite CAIs														
HH 237	l	#1-1, fr	–	–	–	+	+	+	+	+	–	–	–	–
HH 237	l	#1-3	–	–	–	–	+	+	+	+	–	–	–	–
HH 237	l	#4-3	–	–	–	–	+	+	+	–	–	–	–	+
HH 237	AM	#2	–	–	–	–	+	+	+	–	–	–	–	+
HH 237	ss	#3, fr	–	–	–	–	+	+	+	–	–	–	–	–
HH 237	ss	#4, fr	–	–	–	–	+	+	+	–	–	–	–	–
HH 237	ls	#8	–	–	–	–	+	+	+	–	–	–	–	+
HH 237	s	#4, fr	–	–	–	–	–	+	+	–	–	–	–	–
HH 237	AM	#3	–	–	–	–	–	+	+	–	–	–	–	+

Chondrite	ps	chd no.	hb	grs	pv	mel	sp	cpx	px	fo	mes
Al-diopside-rich chondrules											
HH 237	ls	#6, fr	–	–	–	–	+	+	–	+	–
HH 237	ls	#2, fr	–	–	–	–	+	+	–	+	–
HH 237	ls	#3	–	–	–	–	+	+	–	+	–
HH 237	ss	#5	–	–	–	–	+	+	–	+	–
QUE 94411	6	#2	–	–	–	–	–	+	+	–	–
QUE 94627	4	#B	–	–	–	–	–	+	+	+	+
QUE 94627	4	#F	–	–	–	–	–	+	+	+	+
HH 237	ls	#4	–	–	–	–	–	+	+	+	+
HH 237	AM	#5a	–	–	–	–	–	+	–	+	+

Abbreviations: hb = hibonite; grs = grossite; mel = melilite; pv = perovskite; sp = spinel; cpx = Al,(Ti)-diopside; px = low-Ca pyroxene; an = anorthite; mes = mesostasis; fo = forsterite; ps = polished section number; no = CAI/chondrule number; fr = fragment.

INTRODUCTION

Hammadah al Hamra (HH) 237 and Queen Alexandra Range (QUE) 94411, paired with QUE 94627, are metal-rich meteorites (60–70 vol% of FeNi-metal), which also contain calcium-aluminum-rich inclusions (CAIs), Al-diopside-rich chondrules, barred-olivine, and cryptocrystalline chondrules (Zipfel *et al.*, 1998; Weisberg *et al.*, 1998, 2001; Campbell *et al.*, 2000; Meibom *et al.*, 2000; Petaev *et al.*, 2001; Krot *et al.*, 2001). They show several unique, mineralogical and chemical signatures, which are largely shared with the CH chondrites and two other metal-rich chondrites, Bencubbin and Weatherford. (1) They have much higher metal/silicate ratios than any other chondrite group; (2) fine-grained matrix material associated with chondrules, metal and CAIs is largely absent; (3) nitrogen isotopic compositions show extreme enrichments in ^{15}N; and (4) they are highly depleted in moderately volatile elements (Na, K, S). Based on these observations and the fact that CR and CH chondrites and several ungrouped metal-rich chondrites (HH 237, QUE 94411/94627, Bencubbin, Weatherford) have similar bulk O-isotopic compositions, these meteorites have been grouped together in the CR clan (Weisberg *et al.*, 1998, 2001).

Although rare, heavily-hydrated matrix lumps (often called dark inclusions or dark clasts), mineralogically similar to those present in the CH and CR chondrites (*e.g.*, Grossman *et al.*, 1988; Scott, 1988; Bischoff *et al.*, 1993a,b; Endreβ *et al.*, 1994), were identified in QUE 94411/94627 and HH 237, chondrules and CAIs in these meteorites show no evidence for aqueous alteration (Greshake *et al.*, 2000; Krot *et al.*, 2001). Based on the presence of metastable, compositionally zoned metal grains in these meteorites, it was concluded that these rocks escaped thermal metamorphism above 300 °C (Meibom *et al.*, 2000; Weisberg *et al.*, 2001). The primitive characteristics of QUE 94411/94627 and HH 237 make them potentially important for understanding high-temperature nebular processes.

Wasson and Kallemeyn (1990) and Wasson (2000, pers. comm.) questioned the classification of the QUE 94411/94627, HH 237 and CH chondrites as primitive carbonaceous chondrites and suggested that their unusual mineralogical and chemical characteristics could have resulted from melting, vaporization, outgassing, condensation, and size-sorting in a cloud of impact ejecta on the CR parent asteroid. In this model, CAIs are conceived as foreign objects that were randomly mixed in the ejecta during late stages of the impact process.

In this paper, we describe the mineralogy, petrography and oxygen isotopic compositions of 40 CAIs and 7 Al-diopside-rich chondrules in QUE 94411/94627 and HH 237 (Table 1). We compare them to CAIs and Al-rich chondrules in other chondrite groups and discuss their crystallization histories and relationship to the barred-olivine chondrules in QUE 94411/94627 and HH 237. Additionally, we argue that the characteristics of the CAIs and Al-diopside-rich chondrules in QUE 94411/94627 and HH 237 are inconsistent with an impact origin for these metal-rich chondrites.

ANALYTICAL PROCEDURES

Polished sections of Bencubbin (USNM 5717-1) HH 237 [l, s, ss, ls, AMNH 4956-2 (AM)] and QUE 94411 (4, 6, 7, 9) paired with QUE 94627 (4) were studied using optical microscopy, backscattered electron (BSE) imaging, x-ray elemental mapping, electron probe microanalysis (EPMA), laser ablation inductively-coupled plasma mass spectrometry (LA-ICP-MS), and ion probe microanalysis. BSE images were obtained with a Zeiss DSM-962 scanning electron microscope (SEM) using a 15 kV accelerating voltage and 1–2 nA beam current. Electron probe microanalyses were performed with a Cameca SX-50 electron microprobe using a 15 kV accelerating voltage, 10–20 nA beam current, beam size of ~1–2 μm and wavelength dispersive x-ray spectroscopy. For each element, counting times on both peak and background were 30 s (10 s for Na and K). Matrix effects were corrected using PAP procedures. Representative analyses are shown in Tables 2 to 6. The element detection limits with the Cameca SX-50 were (in wt%): SiO_2, Al_2O_3, MgO, V_2O_5, 0.03; TiO_2, CaO, K_2O, 0.04; Na_2O, 0.05; Cr_2O_3, 0.06; MnO, 0.07; FeO, 0.08.

X-ray elemental maps with resolution of 2–5 μm/pixel were acquired using five spectrometers of the Cameca microprobe at 15 kV accelerating voltage, 50–100 nA beam current and ~1–2 μm beam size. The elemental maps in Mg, Ca, and Al Kα were combined using a RGB-color scheme. The obtained false color maps were used to identify Al-rich objects larger than 5–10 μm in apparent diameter.

Bulk compositions of CAIs were calculated based on modal mineralogy (estimated from BSE images and x-ray elemental maps) and mineral compositions (Table 7). The average analytical errors resulted from uncertainties in the modal mineralogy estimates were ~5–10 rel%. Bulk compositions of chondrules were measured using defocused (10 μm) electron beam analysis (Table 8). The analytical errors for the bulk compositions of the Al-diopside-rich and barred-olivine chondrules were (in wt%): SiO_2, CaO, MgO, <2; TiO_2, <0.2; Al_2O_3, FeO, <1; Cr_2O_3, <0.3; MnO, Na_2O, and K_2O were generally below the detection limits of electron microprobe analysis. The analytical errors for the bulk compositions of the cryptocrystalline chondrules were <0.2 wt% for all elements analyzed. Trace elements in CAIs and chondrules were analyzed using the Natural History Museum VG PlasmaQuad LA-ICP-MS, with a 213 nm laser; typical pit sizes were 50 to 90 μm; analytical errors were ~10–20 rel% (for details see Russell *et al.*, 2000b). Results are shown in Table 9.

Oxygen isotopic ratios were measured *in situ* with the UCLA Cameca IMS 1270 ion microprobe operating at a high mass resolution with a beam spot size of ~10 μm (for details see McKeegan *et al.*, 1998a; Simon *et al.*, 2000). Instrumental mass fractionation was corrected by using a Burma spinel and San Carlos

TABLE 2. Representative microprobe analyses and structural formulae of hibonite, grossite, perovskite, and forsterite in CAIs in Hammadah al Hamra 237.

Chondrite	ps	CAI no.	core [rim] mineralogy	min	SiO_2	TiO_2	Al_2O_3	Cr_2O_3	FeO	MgO	CaO	Total	Si	Ti	Al	Cr	Fe	Mg	Ca	Total
HH 237	l	#4-1	hb+mel+pv [sp+cpx+fo]	hb	0.13	1.6	89.0	<0.06	0.05	0.73	8.3	99.9	0.014	0.138	11.714	–	0.005	0.122	0.996	12.991
HH 237	l	#4-1	hb+mel+pv [sp+cpx+fo]	fo, rim	42.6	<0.04	0.08	0.11	0.90	56.4	0.55	100.6	0.997	–	0.002	0.002	0.018	1.968	0.014	3.001
HH 237	s	#1	grs [mel+sp+cpx]	grs	0.24	0.16	77.9	<0.06	0.19	0.04	21.6	100.1	0.011	0.005	3.971	–	0.007	0.002	1.000	4.999
HH 237	ss	#1	mel+pv+sp+cpx [fo]	pv	0.14	56.5	0.31	0.06	0.30	0.05	40.0	97.4	0.003	0.988	0.008	0.001	0.006	0.002	0.996	2.004
HH 237	l	#4-2	mel+sp+cpx [fo]	fo, rim	41.9	<0.04	0.11	0.07	1.3	55.0	0.99	99.4	0.996	–	0.003	0.001	0.026	1.948	0.025	3.001
HH 237	s	#3	sp+cpx [fo]	fo, rim	42.5	<0.04	0.06	0.20	1.5	56.0	0.51	100.8	0.996	–	0.002	0.004	0.030	1.956	0.013	3.000
HH 237	l	#4-3	sp+cpx+fo [fo]	fo, core	42.4	<0.04	0.08	<0.06	0.29	55.8	0.89	99.5	1.001	–	0.002	–	0.006	1.963	0.022	2.997
HH 237	AM	#2	sp+cpx+fo+an [fo]	an	44.4	0.10	35.0	<0.06	0.89	0.64	19.4	100.4	2.048	0.003	1.903	–	0.035	0.044	0.961	4.998
HH 237	l	#1-3	sp+cpx+fo+an	fo	42.5	<0.04	0.04	<0.06	0.83	55.9	0.55	99.8	1.001	–	0.001	–	0.016	1.962	0.014	2.997

Abbreviations: min = mineral; other abbreviations as in Table 1; structural formulae based on 19 O (hb), 4 O (fo), 7 O (grs), 3 O (pv), and 8 O (an).

TABLE 3. Representative microprobe analyses of melilite in CAIs in Hammadah al Hamra 237 and QUE 94411/94627.

Chondrite	ps	CAI no.	core [rim] mineralogy	SiO_2	TiO_2	Al_2O_3	Cr_2O_3	FeO	MnO	MgO	CaO	Na_2O	K_2O	Total	Åk
HH 237	AM	#4	hb+mel+pv [mel+cpx]	22.8	0.13	34.6	<0.06	1.1	<0.07	0.88	40.0	<0.05	<0.04	99.5	6.0
HH 237	ls	#11	hb+sp+pv [mel+cpx]	24.4	0.09	31.8	<0.06	1.3	<0.07	2.7	39.2	<0.05	<0.04	99.4	17.5
HH 237	s	#1	grs+pv [mel+sp+cpx]	22.6	0.26	35.3	<0.06	0.26	<0.07	0.77	40.5	<0.05	<0.04	99.7	5.3
QUE 94411	4	#2	mel, fr	23.0	0.11	34.5	<0.06	1.2	<0.07	1.0	40.5	<0.05	<0.04	100.3	6.8
HH 237	ls	#9a	mel [cpx+fo]	22.0	0.17	35.8	<0.06	0.38	0.12	0.61	40.8	<0.05	<0.04	100.0	4.1
HH 237	ss	#2	mel+sp+cpx, fr	22.9	0.14	33.8	<0.06	1.7	<0.07	1.5	38.4	<0.05	<0.04	98.5	9.9
HH 237	ls	#15	mel+sp, fr	24.5	0.05	31.6	<0.06	0.59	<0.07	2.2	38.6	<0.05	<0.04	97.5	14.9
HH 237	AM	#1	mel+sp+cpx [fo]	25.5	<0.04	30.7	<0.06	0.35	<0.07	2.5	40.7	<0.05	<0.04	99.7	17.0
HH 237	ss	#1	mel+sp+cpx+pv [fo]	26.1	0.09	28.8	<0.06	0.25	<0.07	3.1	39.8	<0.05	<0.04	98.1	21.5
QUE 94627	4	C	sp+pv [mel+cpx+an]	28.2	<0.04	26.3	<0.06	0.50	<0.07	4.2	40.8	<0.05	<0.04	100.0	28.8
QUE 94627	4	A	mel+sp+cpx [fo]	33.2	0.07	19.3	<0.06	0.40	<0.07	7.0	40.7	<0.05	<0.04	100.7	47.9
HH 237	ls	#9	mel+sp+cpx [fo]	32.1	0.04	18.7	<0.06	0.13	<0.07	7.0	40.1	<0.05	<0.04	97.9	48.6
HH 237	ls	#7	mel+sp+cpx [fo]	36.1	<0.04	11.6	<0.06	0.69	<0.07	9.7	38.8	<0.05	<0.04	96.8	67.8
HH 237	l	#1-1	cpx+sp+mel+fo+an, fr	38.7	<0.04	7.8	<0.06	0.69	<0.07	10.9	40.5	<0.05	<0.04	98.7	77.9

Abbrevaitions as in Table 1; in CAI #4, only rim melilite was analyzed.

TABLE 4. Representative microprobe analyses and structural formulae of pyroxenes (based on 6 O) in CAIs in Hammadah al Hamra 237 and QUE 94411/94627.

Chondrite	ps	CAI no.	CAI [rim] mineralogy	SiO_2	TiO_2	Al_2O_3	Cr_2O_3	FeO	MgO	CaO	Total	Si	Ti	Al	Cr	Fe	Mg	Ca	Total	Fs	Wo
HH 237	l	#4-1	hb+mel+pv [sp+cpx+fo]	45.2	1.6	13.2	0.10	1.0	13.1	24.2	98.4	1.669	0.045	0.574	0.003	0.031	0.719	0.956	3.997	1.8	56.1
HH 237	l	#4-1	hb+mel+pv [sp+cpx+fo]	39.1	3.2	20.5	0.10	1.8	9.7	24.8	99.2	1.450	0.089	0.895	0.003	0.055	0.535	0.984	4.010	3.5	62.5
HH 237	ss	#1	mel+pv+sp+cpx [fo]	24.9	17.1	25.8	0.16	0.42	3.5	24.2	96.1	0.978	0.505	1.194	0.005	0.014	0.203	1.017	3.916	1.1	82.4
HH 237	ss	#1	mel+pv+sp+cpx [fo]	38.5	5.8	20.3	0.13	0.10	9.1	24.9	99.0	1.423	0.162	0.886	0.004	0.003	0.504	0.988	3.970	0.2	66.1
QUE 94627	4	A	mel+sp+cpx [fo]	38.9	5.9	20.1	0.11	2.2	9.0	25.0	101.2	1.419	0.162	0.863	0.003	0.067	0.490	0.979	3.983	4.4	63.7
HH 237	AM	#1	mel+sp+cpx [fo]	45.4	1.5	14.8	0.13	1.0	12.7	24.9	100.4	1.642	0.041	0.630	0.004	0.031	0.685	0.967	4.000	1.9	57.5
HH 237	AM	#1	mel+sp+cpx [fo]	42.8	1.1	19.3	0.07	0.44	10.9	25.3	99.8	1.556	0.029	0.825	0.002	0.013	0.590	0.984	3.999	0.8	62.0
HH 237	ls	#9	mel+sp+cpx [fo]	42.5	0.95	17.8	0.15	0.78	11.5	24.0	97.8	1.577	0.026	0.780	0.004	0.024	0.637	0.955	4.003	1.5	59.1
HH 237	ls	#9	mel+sp+cpx [fo]	33.3	9.5	20.1	0.09	3.0	7.9	23.5	97.3	1.281	0.274	0.911	0.003	0.097	0.451	0.968	3.985	6.4	63.8
HH 237	l	#1-2	sp+cpx [fo]	42.6	1.2	16.0	0.05	3.2	12.1	23.4	98.5	1.585	0.032	0.704	0.001	0.101	0.671	0.933	4.028	5.9	54.7
HH 237	l	#1-2	sp+cpx [fo]	39.9	0.45	23.3	<0.06	1.9	8.9	25.0	99.6	1.465	0.012	1.009	–	0.059	0.489	0.981	4.015	3.9	64.2
HH 237	l	#3-1	sp+cpx [fo]	47.5	2.0	9.5	0.09	2.3	15.1	23.9	100.4	1.729	0.054	0.407	0.003	0.071	0.816	0.930	4.011	3.9	51.2
HH 237	l	#3-1	sp+cpx [fo]	42.7	3.9	15.2	0.13	1.7	12.3	24.3	100.2	1.562	0.106	0.655	0.004	0.052	0.670	0.950	4.000	3.1	56.8
HH 237	ls	#7	mel+sp+cpx [fo]	39.8	2.3	19.9	<0.06	0.63	10.1	24.3	97.1	1.493	0.066	0.881	–	0.020	0.562	0.976	3.998	1.3	62.6
QUE 94411	4	#1	sp+cpx [fo]	51.3	1.1	5.5	0.06	0.07	18.2	23.5	99.8	1.849	0.031	0.232	0.002	0.002	0.979	0.908	4.002	0.1	48.1
QUE 94411	4	#1	sp+cpx [fo]	47.3	2.3	9.7	0.12	0.81	15.3	23.9	99.3	1.728	0.062	0.415	0.004	0.025	0.832	0.934	3.999	1.4	52.2
HH 237	ls	#5	cpx [fo]	33.4	7.0	23.8	0.24	1.6	6.5	24.0	96.5	1.282	0.202	1.075	0.007	0.051	0.371	0.986	3.974	3.6	70.0
HH 237	ls	#5	cpx [fo]	40.7	3.2	16.5	0.09	2.3	10.4	24.1	97.3	1.539	0.091	0.733	0.003	0.074	0.587	0.975	4.001	4.5	59.6
HH 237	ls	#5	cpx [fo]	46.1	<0.04	11.2	0.15	3.1	13.1	24.1	97.7	1.727	0.001	0.494	0.004	0.096	0.730	0.968	4.021	5.3	54.0
HH 237	ls	#8	sp+cpx+fo [fo]	53.1	0.74	3.2	<0.06	0.75	27.2	12.3	97.2	1.904	0.020	0.134	–	0.022	1.453	0.473	4.006	1.1	24.3
HH 237	ls	#8	sp+cpx+fo [fo]	46.4	2.2	9.2	0.08	1.5	14.7	23.6	97.6	1.730	0.061	0.406	0.002	0.046	0.818	0.942	4.005	2.5	52.2
HH 237	l	#1-1, fr	mel+sp+cpx+an	50.0	0.58	7.2	0.07	0.70	16.0	25.1	99.5	1.819	0.016	0.307	0.002	0.021	0.867	0.978	4.010	1.1	52.4
HH 237	l	#1-1, fr	mel+sp+cpx+an	44.7	0.98	15.7	0.10	0.83	12.3	24.7	99.3	1.631	0.027	0.678	0.003	0.025	0.669	0.967	4.000	1.5	58.2
HH 237	l	#4-3	sp+cpx+fo [fo]	46.1	1.9	12.7	0.15	0.15	13.1	25.1	99.2	1.683	0.053	0.546	0.004	0.005	0.714	0.984	3.988	0.3	57.8
HH 237	l	#4-3	sp+cpx+fo [fo]	42.6	2.3	16.7	0.11	0.60	11.6	24.4	98.3	1.575	0.064	0.728	0.003	0.019	0.637	0.968	3.995	1.1	59.6
HH 237	AM	#2	sp+cpx+fo+an [fo]	50.9	0.53	7.8	<0.06	1.8	18.7	20.4	100.1	1.821	0.014	0.329	–	0.054	0.996	0.783	3.997	2.9	42.7
HH 237	l	#1-3	sp+cpx+fo+an	50.3	1.1	6.6	0.08	0.52	16.6	24.3	99.4	1.828	0.029	0.281	0.002	0.016	0.900	0.945	4.001	0.8	50.8

Abbreviations as in Table 1; MnO, Na_2O, and K_2O are below detection limits of electron probe microanalyses (<0.07, <0.05 and <0.04 wt%, respectively).

TABLE 5. Representative microprobe analyses and structural formulae of pyroxenes (based on 6 O) in Al-diopside-rich chondrules in Hammadah al Hamra 237 and QUE 94411/94627.

Chondrite	ps	Chd. no.	Mineralogy	SiO_2	TiO_2	Al_2O_3	Cr_2O_3	FeO	MgO	CaO	Total	Si	Ti	Al	Cr	Fe	Mg	Ca	Total	Fs	Wo
HH 237	ls	#3	cpx+sp+fo	43.3	1.9	16.4	0.11	1.9	12.4	22.3	98.4	1.598	0.053	0.713	0.003	0.058	0.682	0.883	3.990	3.6	54.4
HH 237	ss	#5	cpx+sp+fo	50.4	0.41	7.0	0.08	0.52	18.5	21.8	98.7	1.830	0.011	0.300	0.002	0.016	0.999	0.850	4.008	0.8	45.6
HH 237	ss	#5	cpx+sp+fo	43.5	2.4	16.4	0.21	0.53	13.0	22.9	99.0	1.589	0.067	0.705	0.006	0.016	0.708	0.897	3.988	1.0	55.3
HH 237	ls	#2	cpx+sp+fo	50.5	1.1	6.1	0.39	1.2	21.0	17.7	98.0	1.835	0.030	0.261	0.011	0.037	1.136	0.688	3.997	2.0	37.0
HH 237	ls	#2	cpx+sp+fo	45.6	1.6	12.8	0.57	0.84	15.3	21.0	97.7	1.679	0.045	0.556	0.017	0.026	0.837	0.826	3.987	1.5	48.9
HH 237	ls	#6	cpx+sp+fo	45.8	1.3	13.1	0.14	0.95	15.3	21.4	98.0	1.683	0.036	0.565	0.004	0.029	0.839	0.840	3.995	1.7	49.2
HH 237	ls	#6	cpx+sp+fo	50.9	0.69	5.4	0.06	1.1	19.0	20.7	97.8	1.864	0.019	0.231	0.002	0.034	1.038	0.814	4.001	1.8	43.2
HH 237	ls	#4	cpx+px+fo+mes	48.0	0.15	12.9	0.09	0.15	18.0	19.0	98.4	1.729	0.004	0.548	0.003	0.005	0.968	0.734	3.991	0.3	43.0
HH 237	ls	#4	cpx+px+fo+mes	42.5	2.0	16.5	0.74	1.3	12.5	21.5	97.2	1.585	0.055	0.726	0.022	0.042	0.695	0.860	3.985	2.6	53.8
HH 237	ls	#4	cpx+px+fo+mes	52.4	0.46	8.6	0.18	0.50	33.9	1.9	98.0	1.807	0.012	0.351	0.005	0.014	1.745	0.069	4.002	0.8	3.8
HH 237	ls	#4	cpx+px+fo+mes	51.3	0.40	12.0	0.27	0.52	32.8	2.0	99.3	1.748	0.010	0.481	0.007	0.015	1.662	0.073	3.997	0.8	4.2
QUE 94627	4	B	cpx+px+fo+mes	48.6	0.91	13.7	0.07	0.48	18.2	19.4	101.5	1.702	0.024	0.566	0.002	0.014	0.952	0.729	3.988	0.8	43.0
QUE 94627	4	B	cpx+px+fo+mes	51.3	0.25	14.3	0.06	0.55	26.6	8.3	101.5	1.735	0.006	0.569	0.002	0.015	1.341	0.300	3.969	0.9	18.1
QUE 94627	4	F	cpx+px+fo+mes	48.2	1.0	12.5	0.13	0.90	18.3	19.5	100.7	1.708	0.027	0.523	0.004	0.027	0.968	0.741	3.997	1.5	42.7
QUE 94627	4	F	cpx+px+fo+mes	49.6	0.61	12.0	0.10	0.42	32.2	6.3	101.6	1.682	0.016	0.480	0.003	0.012	1.628	0.230	4.050	0.6	12.3
QUE 94411	6	#2	cpx+px	48.4	0.99	11.8	1.1	1.2	19.1	18.8	101.4	1.706	0.026	0.489	0.031	0.036	1.005	0.712	4.005	2.1	40.6
QUE 94411	6	#2	cpx+px	51.5	0.48	14.3	0.33	1.0	27.0	6.3	100.8	1.744	0.012	0.570	0.009	0.029	1.361	0.227	3.952	1.8	14.1

Abbreviations as Table 1; MnO, Na_2O, and K_2O are below detection limits of electron probe microanalyses (<0.07, <0.05 and <0.04 wt%, respectively).

TABLE 6. Representative microprobe analyses of spinel in CAIs in Hammadah al Hamra 237 and QUE 94411/94267.

Chondrite	ps	CAI no.	core [rim] mineralogy	SiO_2	TiO_2	Al_2O_3	Cr_2O_3	FeO	MnO	MgO	CaO	V_2O_5	Total
HH 237	l	#4-1	hb+mel+pv [sp+cpx+fo]	0.36	0.22	71.0	0.10	0.43	<0.07	26.9	0.28	0.15	99.4
HH 237	s	#1	grs [mel+sp+cpx]	0.24	0.26	71.6	0.37	0.63	<0.07	27.6	0.13	0.49	101.2
QUE 94267	4	A	mel+cpx+sp [fo]	0.07	0.49	71.8	0.54	0.27	<0.07	28.2	0.23	0.30	101.8
QUE 94267	4	C	sp [mel+cpx+an]	0.05	0.64	71.7	0.15	0.44	0.03	28.1	0.16	0.10	101.4
HH 237	l	#4-2	mel+sp+cpx [fo]	0.15	0.39	70.5	0.52	0.59	<0.07	27.4	0.09	0.26	99.9
HH 237	l	#1-1	cpx+sp+mel+fo+an, fr	0.05	0.51	70.8	0.26	0.36	<0.07	27.5	0.06	0.82	100.4
HH 237	l	#3-1	sp+cpx [fo]	0.29	0.15	69.9	0.51	1.65	<0.07	27.3	<0.04	0.52	100.3
HH 237	l	#4-3	sp+cpx [fo]	0.16	0.47	70.1	0.68	0.22	<0.07	27.7	<0.04	0.58	99.9
HH 237	s	#3-1	sp+cpx [fo]	0.05	0.22	71.5	0.26	1.0	<0.07	27.8	<0.04	n.a.	100.8
QUE 94411	4	#1	sp+cpx [fo]	0.06	0.24	71.08	0.42	0.22	<0.07	27.8	0.05	0.52	100.4

Abbreviations as in Table 1; n.a. = not analyzed.

TABLE 7. Bulk compositions (normalized to 100%) of CAIs in Hammadah al Hamra 237 and QUE 94411/94627.

Chondrite	ps	CAI no.	core [rim] mineralogy	SiO_2	TiO_2	Al_2O_3	Cr_2O_3	FeO	MnO	MgO	CaO	Na_2O	K_2O
HH 237	l	#4-1	hb+mel+pv [sp+cpx+fo]	14.3	0.86	56.4	<0.06	0.63	<0.07	6.8	21.1	<0.05	<0.04
HH 237	AM	#4	hb+mel+pv [mel+sp+cpx]	12.7	0.81	59.2	<0.06	0.63	<0.07	0.8	25.9	<0.05	<0.04
HH 237	s	#1	grs+pv [mel+sp+cpx]	5.8	0.39	69.1	<0.06	0.31	<0.07	1.2	23.2	<0.05	<0.04
HH 237	ss	#2, fr	mel+pv+sp+cpx	12.3	3.0	50.7	0.13	2.4	<0.07	19.5	11.9	<0.05	<0.04
HH 237	AM	#1	mel+sp+cpx [fo]	15.9	0.60	49.8	0.09	0.66	<0.07	19.4	13.7	<0.05	<0.04
HH 237	ls	#11	sp+hb+pv [mel+cpx]	15.6	5.1	45.1	0.08	1.0	<0.07	15.6	17.4	<0.05	<0.04
HH 237	ls	#7	mel+sp+cpx [fo]	17.7	0.22	44.3	0.24	0.89	<0.07	24.0	12.7	<0.05	<0.04
HH 237	ss	#1	mel+pv+sp+cpx [fo]	23.8	0.91	33.9	0.08	0.26	<0.07	6.7	34.3	<0.05	<0.04
HH 237	ls	#9a	mel [cpx+fo]	24.9	0.22	32.1	<0.06	0.45	0.10	4.5	37.7	<0.05	<0.04
HH 237	ls	#9	mel+sp+cpx [fo]	27.5	2.1	29.9	0.14	0.64	<0.07	12.7	27.0	<0.05	<0.04
QUE 94627	4	#A	mel+sp+cpx [fo]	27.2	1.1	29.5	0.14	0.70	<0.07	14.8	26.5	<0.05	<0.04
HH 237	ls	#14	mel+pv+sp+cpx [fo]	25.8	3.2	27.7	0.10	1.1	<0.07	14.6	27.5	<0.05	<0.04
HH 237	ls	#1-1	mel+sp+cpx+an	37.6	0.69	24.3	0.12	0.70	<0.07	17.4	19.2	<0.05	<0.04
HH 237	l	#4-2	cpx+sp [fo]	24.0	2.0	39.9	0.28	0.57	<0.07	20.0	13.2	<0.05	<0.04
HH 237	l	#1-2	cpx+sp [fo]	27.4	0.75	36.6	0.19	1.9	<0.07	17.3	15.8	<0.05	<0.04
HH 237	ls	#8	cpx+sp+fo [fo]	32.5	1.1	27.9	0.14	0.97	<0.07	26.0	11.4	<0.05	<0.04
QUE 94411	6	#1	cpx+sp [fo]	42.5	0.86	9.1	0.11	0.71	<0.07	34.8	12.0	<0.05	<0.04
HH 237	l	#4-3	sp+cpx+fo [fo]	42.4	0.50	4.6	<0.06	0.31	<0.07	45.7	6.4	<0.05	<0.04

Abbreviations as in Table 1.

TABLE 8. Bulk compositions (normalized to 100%) of chondrules in Hammadah al Hamra 237 and QUE 94411/94627.

Chondrite	ps	chd	Type	SiO_2	TiO_2	Al_2O_3	Cr_2O_3	FeO	MnO	MgO	CaO	Na_2O
QUE 94411	6	#9	CC	52.9	<0.03	<0.04	0.68	1.4	<0.07	45.0	<0.04	<0.05
HH 237	l	#2	CC	54.7	<0.03	<0.04	0.64	0.73	<0.07	43.8	<0.04	<0.05
QUE 94411	6	#7	CC	55.0	<0.03	<0.04	0.69	1.1	<0.07	43.1	<0.04	<0.05
HH 237	l	#11	CC	54.9	<0.03	0.22	0.71	0.71	<0.07	43.2	0.16	<0.05
HH 237	l	#17	CC	52.2	0.05	0.67	0.44	1.4	<0.07	44.5	0.70	<0.05
QUE 94411	6	#12	CC	53.9	0.06	0.77	0.73	1.0	<0.07	42.8	0.69	<0.05
QUE 94411	6	#8	CC	53.6	0.09	1.4	0.58	1.2	<0.07	41.9	1.2	<0.05
QUE 94411	6	#5	CC	53.3	0.08	1.7	0.66	0.94	0.08	41.9	1.3	<0.05
HH 237	l	#10	CC	53.0	0.10	1.9	0.77	2.5	0.22	39.9	1.6	<0.05
HH 237	l	#13	CC	52.2	0.17	3.7	0.77	3.8	0.27	36.0	2.9	0.10
QUE 94411	6	#10	CC	51.4	0.18	3.8	0.92	2.4	0.11	37.6	3.5	0.08
HH 237	l	#8	CC	52.4	0.18	4.2	0.74	0.80	<0.07	38.2	3.4	0.07
HH 237	l	#12	CC	52.2	0.20	4.6	0.77	2.2	0.38	36.1	3.3	0.28
QUE 94411	6	#6	BO	52.1	0.27	5.8	0.84	2.8	<0.07	33.4	4.7	<0.05
QUE 94411	6	#1	BO	48.7	0.19	7.0	0.58	2.9	0.25	35.9	4.4	0.06
HH 237	l	#7	BO	45.9	0.37	9.3	0.44	5.4	<0.07	31.5	7.0	<0.05
HH 237	l	#14	BO	46.3	0.42	10.1	0.60	4.3	<0.07	30.4	7.7	0.09
HH 237	l	#8	BO	47.8	0.40	10.5	0.41	2.6	<0.07	30.8	7.4	<0.05
HH 237	l	#16	BO	46.3	0.44	10.6	0.45	3.9	<0.07	30.6	7.6	0.06
HH 237	l	#9	BO	46.3	0.44	10.8	0.47	3.6	<0.07	30.4	8.0	<0.05
QUE 94411	6	#3	BO	47.7	0.41	11.0	0.43	2.2	<0.07	30.5	7.6	0.06
QUE 94411	6	#2	BO	47.6	0.40	11.1	0.48	3.5	<0.07	29.4	7.5	<0.05
HH 237	l	#3	BO	44.8	0.48	12.2	0.28	2.4	<0.07	32.5	7.2	0.09
QUE 94411	6	#11	BO	44.8	0.48	12.2	0.28	2.4	<0.07	32.5	7.2	0.09
QUE 94411	6	#2	BO	48.8	0.47	12.3	0.33	1.6	<0.07	28.5	9.2	<0.05
HH 237	l	#15	BO	44.7	0.54	14.0	0.32	4.9	<0.07	26.6	8.8	0.09
QUE 94627	4	#F	Al-di	49.3	0.77	12.8	0.12	1.6	<0.07	24.3	11.7	0.21
QUE 94627	4	#B	Al-di	48.1	0.78	13.8	0.08	1.6	<0.07	20.5	15.2	0.08
HH 237	MW	#5a	Al-di	46.2	1.1	16.7	0.10	2.3	<0.07	14.9	18.6	0.05

Abbreviations as in Table 1; BO = barred olivine chondrule; CC = cryptocrystalline chondrule; and Al-di = Al-diopside-rich chondrule.

TABLE 9. Concentrations of rare earth elements (in ppm) in CAIs and chondrules from HH 237 and QUE 94411.

Chondrite	Chd. type	Chd. no.	La	Ce	Pr	Nd	Sm	Eu	Gd	Tb	Dy	Ho	Er	Tm	Yb	Lu
HH 237	CAI	#4-1	30.61	48.19	11.35	61.80	18.77	1.76	22.97	4.88	32.42	5.34	12.54	2.63	3.46	0.96
QUE 94411	CAI?	#52	3.16	9.34	1.30	6.34	1.78	0.83	2.07	0.49	3.02	0.66	2.21	0.32	2.41	0.47
HH 237	CAI	#1-1	2.90	8.90	1.55	7.88	3.18	0.54	3.75	0.78	4.80	1.04	3.05	0.53	3.66	0.56
HH 237	CAI	#4-2	2.42	11.26	1.88	9.99	3.91	0.34	3.37	0.70	5.00	0.98	2.75	0.56	3.46	0.39
HH 237	BO	#7	3.32	7.49	1.20	6.09	2.08	0.75	2.85	0.53	3.85	0.86	2.59	0.42	2.22	0.41
HH 237	BO†	#14	2.92	6.19	1.07	5.45	1.83	0.68	2.42	0.46	3.17	0.70	2.10	0.32	2.05	0.32
HH 237	BO†	#15	1.99	4.68	0.70	3.42	1.05	0.51	1.29	0.24	1.61	0.34	1.09	0.16	1.03	0.17
HH 237	BO†	#3	1.73	4.08	0.64	3.13	1.05	0.40	1.50	0.30	2.08	0.45	1.40	0.21	1.16	0.22
QUE 94411	BO†	#11	1.60	3.47	0.59	3.06	0.99	0.38	1.20	0.23	1.63	0.35	1.05	0.16	1.05	0.16
QUE 94411	BO	#53	1.13	2.78	0.46	2.26	0.82	0.33	0.87	0.19	1.34	0.27	0.79	0.12	0.83	0.09
QUE 94411	BO†	#6	0.94	2.57	0.37	1.79	0.57	0.25	0.62	0.14	0.81	0.17	0.54	0.08	0.52	0.08
QUE 94411	BO†	#10	0.50	1.53	0.20	1.05	0.30	0.12	0.42	0.09	0.57	0.15	0.47	0.07	0.38	0.08
HH 237	CC	#13†	0.63	1.71	0.23	1.17	0.40	0.16	0.52	0.10	0.75	0.15	0.46	0.07	0.45	0.07
QUE 94411	CC	#17	0.36	1.24	0.10	0.77	0.29	0.21	0.31	<0.06	0.27	0.05	<0.26	<0.04	<0.28	0.04
QUE 94411	CC	#8	0.34	1.45	0.16	0.69	0.23	0.09	0.18	0.05	0.26	0.05	0.15	0.03	0.29	0.02
QUE 94411	CC	#12	0.27	1.02	0.11	0.61	<0.51	0.12	0.27	0.05	0.29	0.05	<0.22	<0.04	0.20	<0.03
HH 237	CC*	#5	0.27	0.63	0.07	<0.52	0.38	<0.11	<0.24	<0.06	<0.12	0.09	<0.16	<0.04	<0.21	<0.05
QUE 94411	CC*	#2	0.24	0.60	0.08	0.53	<0.24	0.12	0.15	<0.05	0.23	<0.04	<0.17	<0.05	0.26	<0.04
QUE 94411	CC	#5	0.21	0.76	0.09	0.37	0.14	0.05	0.15	<0.03	0.19	0.04	0.13	0.03	0.17	0.02
HH 237	CC	#50	0.13	0.33	0.05	0.25	0.09	0.03	0.11	0.02	0.15	0.03	0.10	0.02	0.10	0.02
HH 237	CC	#17	0.07	1.01	0.04	0.15	<0.05	0.05	<0.05	<0.02	0.08	0.02	0.06	<0.01	0.08	<0.01
QUE 94411	CC	#9	0.02	0.07	0.01	0.03	<0.01	0.01	<0.01	0.00	0.01	0.00	0.01	0.00	<0.01	0.00
QUE 94411	CC	#7	0.01	0.12	0.01	<0.13	<0.06	<0.02	<0.05	<0.01	<0.05	<0.01	<0.05	<0.01	<0.03	<0.01

Abbreviations: CC = cryptocrystalline chondrules; BO = barred olivine chondrules; CAI = calcium-aluminum-rich inclusions.
*Chondrules in zoned FeNi-metal grains.
†Average of two analyses.

TABLE 10. Oxygen-isotopic compositions of CAIs and chondrules in Hammadah al Hamra 237 and QUE 94627.

Chondrite	ps	CAI/Chd. no.	core [rim] mineralogy	min	pt	$\delta^{18}O$ (‰)	1σ (‰)	$\delta^{17}O$ (‰)	1σ (‰)	$\Delta^{17}O$ (‰)	1σ (‰)
HH 237	AM	#4	hb+mel+pv [sp+mel+cpx]	hb+mel	4	−12.98	1.46	−16.72	1.21	−9.98	1.17
HH 237	AM	#4	hb+mel+pv [sp+mel+cpx]	hb+mel	5	−12.14	1.58	−16.20	1.22	−9.89	1.22
HH 237	s	#1	grs [sp+mel+cpx]	grs	7	−11.87	1.56	−13.33	1.12	−7.16	1.11
QUE 94627	4	#C	sp+pv [mel+cpx+an]	sp+cpx+an	C	−17.36	1.97	−18.49	1.28	−9.46	1.39
QUE 94627	4	#A	mel+cpx+sp [fo]	mel	1	−10.99	2.03	−15.35	2.03	−9.63	1.50
QUE 94627	4	#A	mel+cpx+sp [fo]	mel	4	−5.55	1.91	−11.46	1.98	−8.57	1.39
QUE 94627	4	#A	mel+cpx+sp [fo]	mel	7	−8.49	1.84	−13.64	2.04	−9.22	1.44
QUE 94627	4	#A	mel+cpx+sp [fo]	mel	A1	−10.46	2.00	−13.97	1.00	−8.53	1.15
QUE 94627	4	#A	mel+cpx+sp [fo]	mel	A2	−11.19	1.94	−15.80	1.20	−9.98	1.30
QUE 94627	4	#A	mel+cpx+sp [fo]	mel	A3	−10.27	1.85	−14.05	0.91	−8.71	1.00
QUE 94627	4	#A	mel+cpx+sp [fo]	cpx	3	−11.89	2.27	−15.73	2.12	−9.54	1.70
QUE 94627	4	#A	mel+cpx+sp [fo]	sp	2	−12.46	1.98	−15.19	2.02	−8.71	1.46
QUE 94627	4	#A	mel+cpx+sp [fo]	sp/fo	6	−11.35	2.05	−14.59	2.20	−8.69	1.73
HH 237	s	#2	cpx+sp, fr	cpx	8	−10.20	1.51	−14.37	1.12	−9.07	1.10
HH 237	s	#3	cpx+sp [fo]	cpx	9	−5.61	1.49	−9.16	1.26	−6.24	1.24
HH 237	s	#3	cpx+sp [fo]	sp	10	−9.79	1.63	−13.16	1.11	−8.06	1.13
HH 237	AM	#3	cpx+fo [fo]	cpx	6	−13.54	1.52	−19.18	1.13	−12.14	1.11
QUE 94627	4	#B	Al-diopside-rich chondrule	cpx	B	−8.45	1.98	−10.90	0.92	−6.50	1.08
QUE 94627	4	#F	Al-diopside-rich chondrule	cpx	F	−4.29	1.83	−9.14	1.10	−6.91	1.16
QUE 94627	4	#1	CC-chondrule	cpx	5	0.28	1.83	−2.89	1.99	−3.04	1.37

Abbreviations as in Table 1; pt = point, min = mineral.

olivine standards (McKeegan *et al.*, 1997); under our analytical conditions possible matrix effects between spinel and the Fe-poor minerals analyzed here are <1–2‰/amu (1σ). The precision and accuracy for a single analysis of each individual spot is in the range 1–2‰ for both $\delta^{17}O$ and $\delta^{18}O$. Results are shown in Table 10. Following isotopic analyses, each CAI was examined by SEM to verify the locations of the sputtered craters and the mineralogy of the phases analyzed.

RESULTS

Calcium-Aluminum-Rich Inclusions: Mineralogy and Petrography

Refractory inclusions are a minor (<1 vol%), but ubiquitous constituent in QUE 94411/94627 and HH 237 (Table 1; Fig. 1). No CAIs were found in Bencubbin or Weatherford (Zipfel *et al.*, 1998; Weisberg *et al.*, 1998, 2001; Krot *et al.*, 2000a). The CB CAIs and CAI fragments, ~50–400 μm in apparent diameter, have rounded to irregular shapes and compact textures; fluffy-type inclusions are very rare. Based on mineralogy, the refractory inclusions can be divided into seven types: (1) hibonite-rich, (2) hibonite-bearing, spinel-perovskite, (3) grossite-rich, (4) spinel-melilite-pyroxene-anorthite, (5) pyroxene-spinel ± melilite, (6) forsterite-bearing, pyroxene-spinel ± melilite ± anorthite, and (7) amoeboid olivine aggregate (AOA) (Table 1). Secondary alkali-rich minerals (nepheline and sodalite) and phyllosilicates are absent in the CB CAIs and AOA.

(1) Two hibonite-rich CAIs were found. They have cores composed of platy hibonite, interstitial melilite, and minor perovskite (Figs. 2a and 3a–c). The cores are surrounded by multi-layered rims of melilite, Al-diopside, and ±forsterite. Spinel is concentrated in the peripheral portions of the CAIs and appears to be a part of the rims.

(2) One hibonite-bearing, spinel-perovskite CAI was found. It has a massive spinel-hibonite core containing numerous inclusions of perovskite. The core is surrounded by a thick melilite-Al-diopside rim (Fig. 4).

(3) One grossite-rich CAI and a grossite fragment were found. The CAI has a compact grossite core containing tiny inclusions of perovskite; the core is surrounded by a spinel-melilite-Al-diopside rim (Figs. 2b and 3d).

(4) One multicored spinel-rich CAI was found; each core consists of irregularly-shaped spinel ± perovskite and is rimmed by melilite, anorthite, and Al-diopside (Figs. 2d and 3e,f).

(5) The dominant inclusion type is pyroxene-spinel ± melilite; 22 CAIs were found (Table 1). They have rounded shapes and compact, igneous textures. Modal abundances of pyroxene, spinel, and melilite range broadly (Figs. 2c and 5). Spinel occurs as euhedral-to-subhedral grains surrounded by Al-diopside and/or melilite. One of the refractory spherules consists entirely of Al-diopside (Fig. 6a–c). Most pyroxene-spinel ± melilite CAIs are surrounded by forsterite rims of variable thickness.

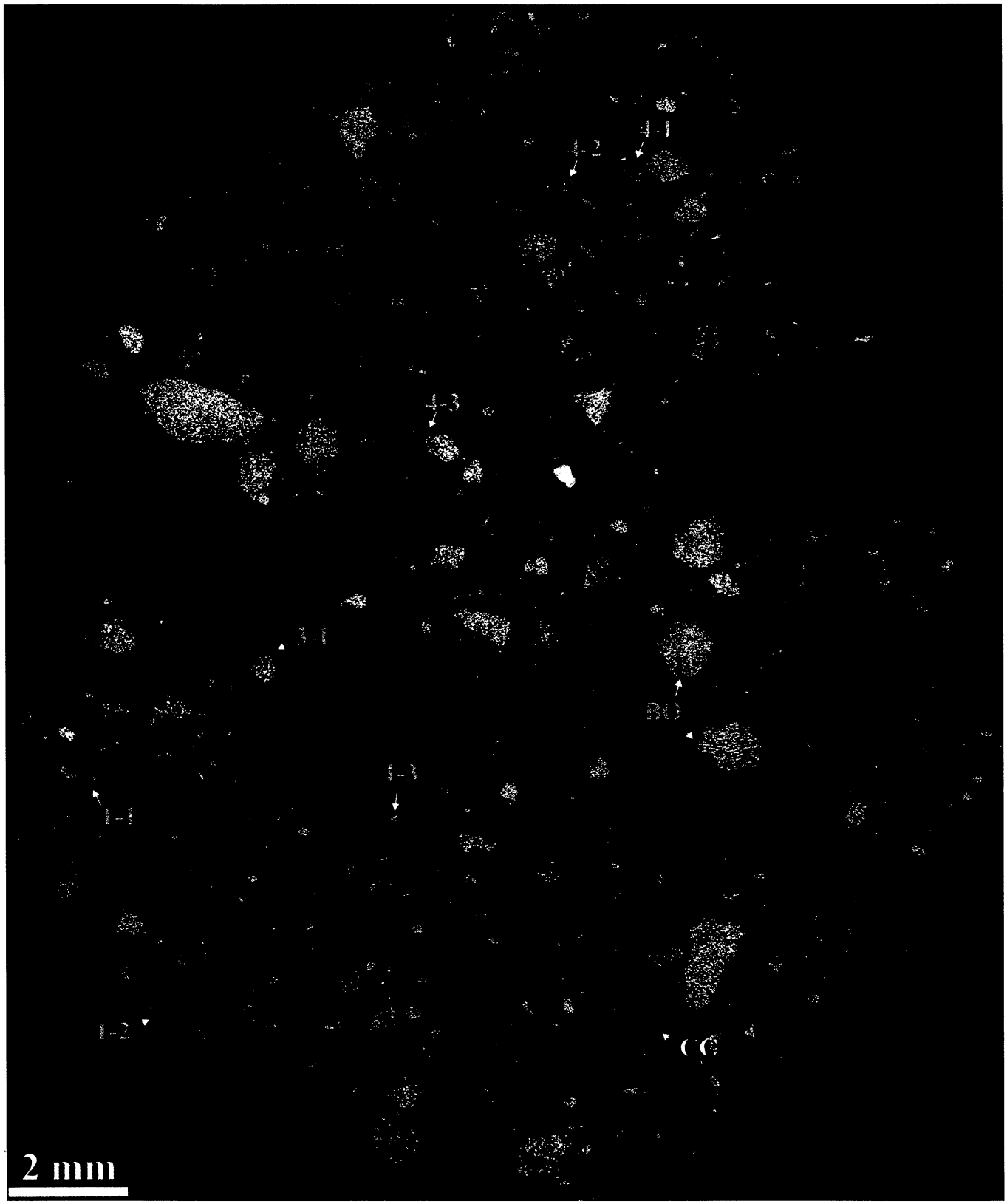

FIG. 1. Combined elemental map in Mg (red), Ca (green) and Al Kα (blue) x-rays of HH 237 (polished section "l"). The meteorite contains rare (<1 vol%) CAIs (labeled by numbers) and two types of chondrules: large, Ca, Al-rich chondrules (bluish) of barred-olivine textures (labeled as "BO") and small Ca, Al-poor chondrules (reddish) of cryptocrystalline textures (labeled as "CC").

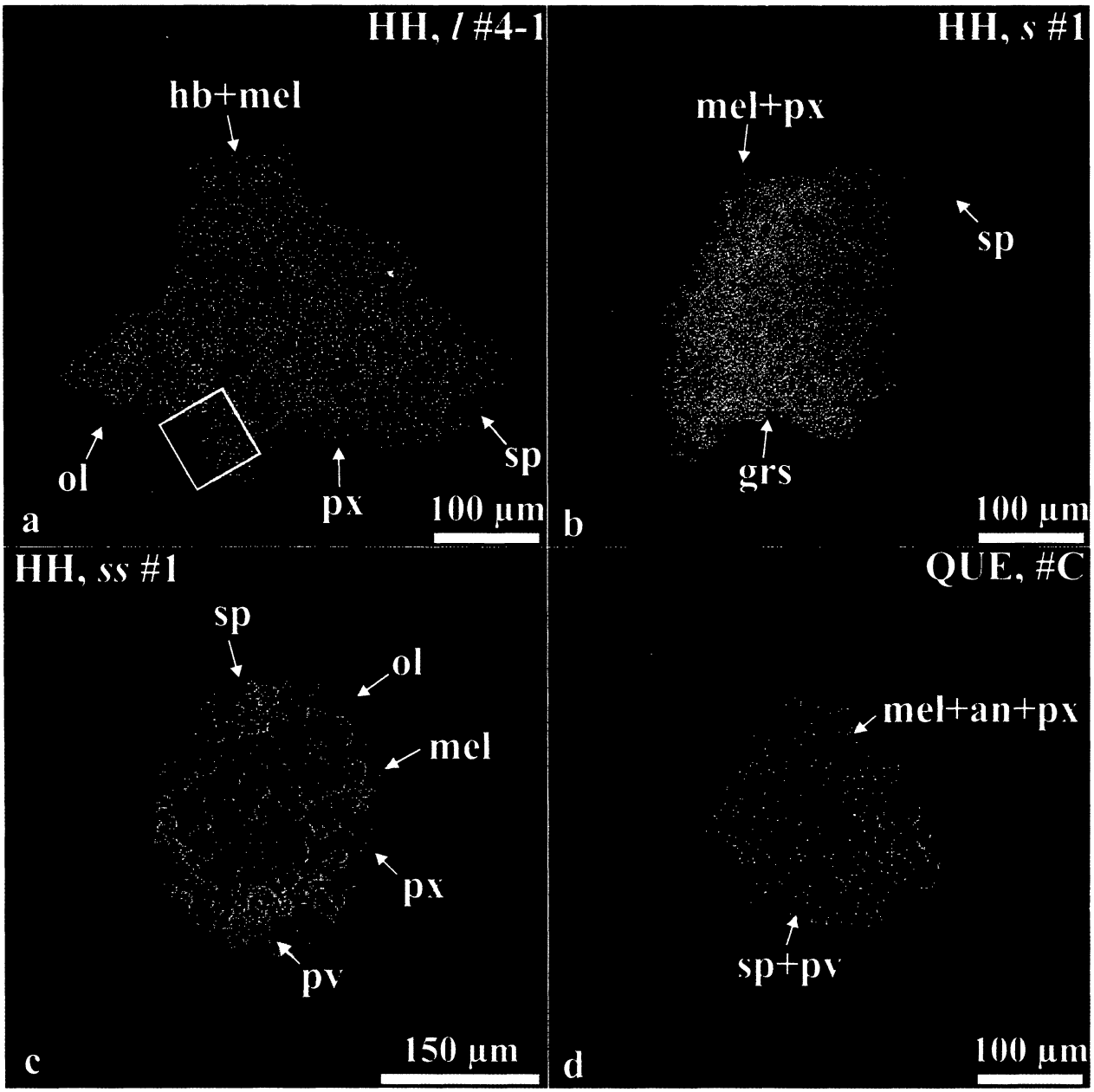

FIG. 2. Combined elemental maps in Mg (red), Ca (green) and Al Kα (blue) x-rays of the pyroxene-poor CAIs from HH 237 and QUE 94411/94627. (a) Compact-type CAI largely composed of hibonite (hb) and melilite (mel); it is surrounded by a multilayered rim of spinel (sp), pyroxene (px), and forsterite (ol). Outlined region is shown in detail in Fig. 3a. (b) Compact-type CAI composed of grossite (grs) and surrounded by a spinel-melilite-pyroxene rim (see also Fig. 3d). (c) Compact type A CAI composed of melilite, fassaitic pyroxene, spinel and minor perovskite; it is surrounded by a pyroxene-forsterite rim. (d) Spinel-rich CAI composed of multiple spinel-perovskite cores surrounded by melilite, anorthite (an), and pyroxene (see also Fig. 3e,f).

(6) Forsterite-bearing CAIs are texturally and mineralogically similar to the pyroxene-spinel ± melilite CAIs described above, but in addition to pyroxene, spinel and melilite (found only in one CAI, #1-1), their cores also contain forsterite (Figs. 6d,e and 7). Eleven forsterite-bearing CAIs were found. Forsterite forms small, anhedral inclusions in Al-diopside and rims host inclusions. One of the forsterite-bearing CAIs is dominated by a coarse-grained forsterite (Fig. 6d). Another CAI is associated with a chondrule-like material composed of anorthite, minor forsterite, and interstitial high-Ca pyroxene and Si-rich mesostasis (Figs. 6e and 7a–d).

(7) One AOA was found. This AOA is texturally and mineralogically similar to AOAs described in CV, CO, and CR carbonaceous chondrites (Hashimoto and Grossman, 1987; MacPherson *et al.*, 1988; Weisberg and Prinz, 1990; Weisberg *et al.*, 1993; Weber and Bischoff, 1997; Chizmadia and Rubin, 2000; Komatsu *et al.*, 2001; Krot, unpubl. data). It consists of a fine-grained refractory material composed of Al-diopside,

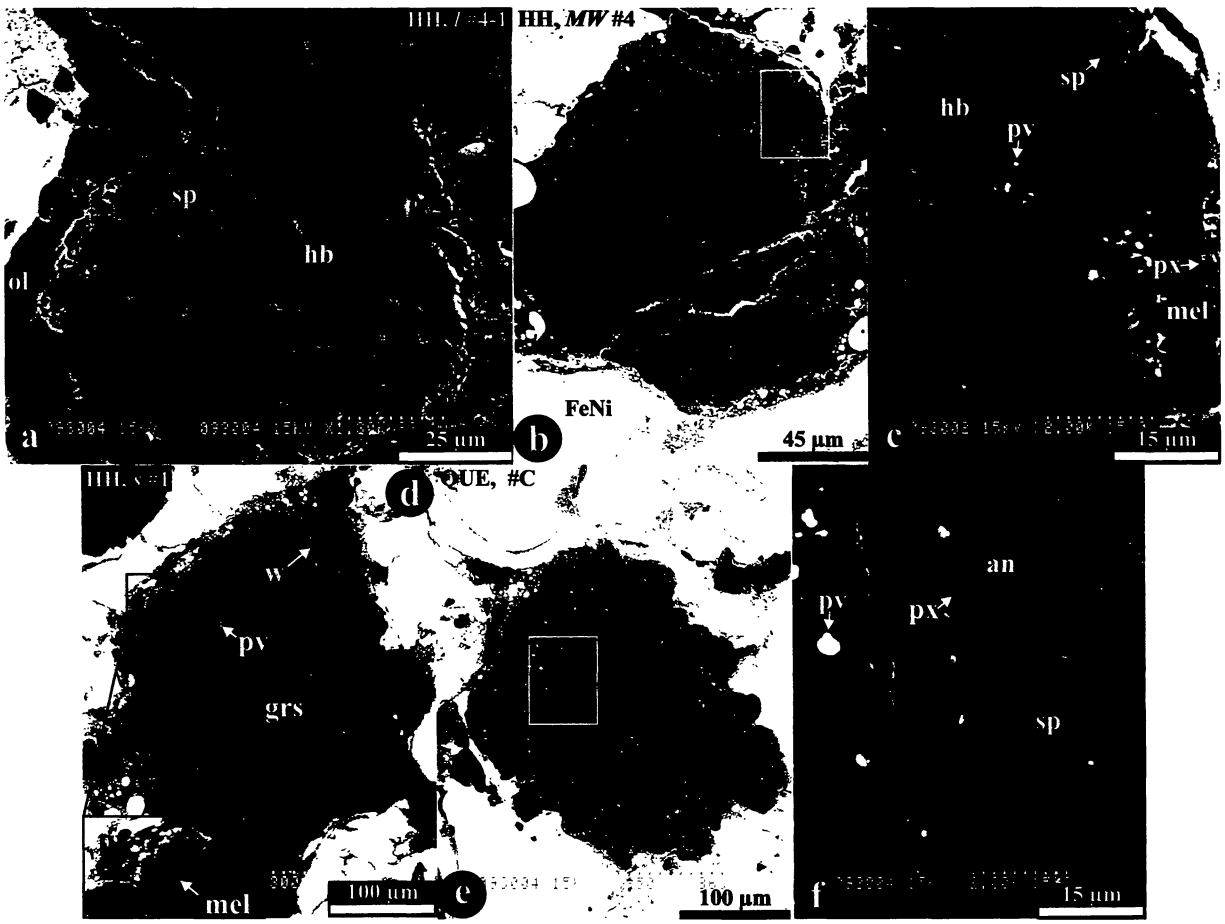

FIG. 3. Backscattered electron images of the pyroxene-poor CAIs from HH 237 and QUE 94411/94627. (a) Hibonite-melilite CAI surrounded by a multilayered rim composed of spinel, pyroxene and forsterite. Spinel is a minor phase inside the CAI. (b, c) Hibonite-rich CAI; melilite, perovskite, spinel, and metal (mt) are minor. The CAI is surrounded by a melilite- pyroxene rim. Region outlined in (b) are shown in detail in (c). (d) Grossite-rich CAI surrounded by a melilite-pyroxene rim (see inset); w = weathering products and holes. (e, f) Spinel-rich CAI composed of multiple spinel-perovskite cores surrounded by melilite, anorthite, and pyroxene. Region outlined in (e) is shown in detail in (f).

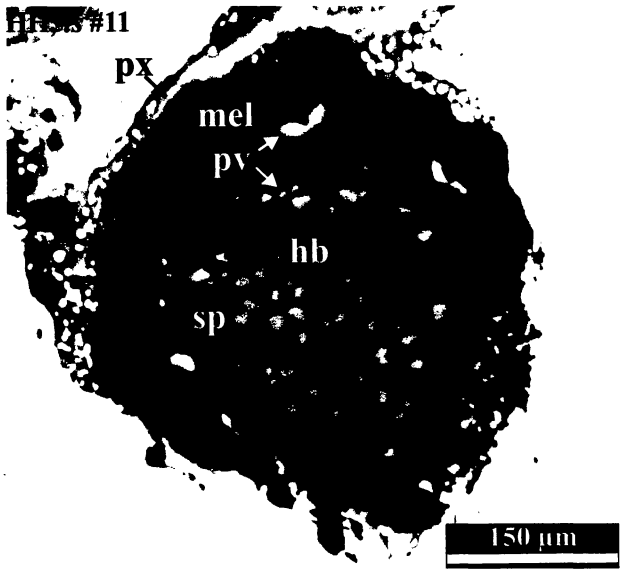

FIG. 4. Backscattered electron image of a spinel-hibonite-perovskite CAI #11 surrounded by a thick melilite-pyroxene rim.

spinel, and anorthite and surrounded by a thick mantle of forsterite containing large FeNi-metal nodules (Fig. 8).

Aluminum-Diopside-Rich Chondrules

Barred-olivine chondrules in HH 237 and QUE 94411/94627 are abundant and often have >10 wt% Al_2O_3 (bulk content); as such they can be designated "Al-rich chondrules" according to the definition by Bischoff and Keil (1984). These chondrules consist of forsterite, Al-rich (high-Ca and low-Ca) pyroxenes, and anorthitic mesostasis; the modal abundances of these minerals range broadly (Fig. 9). In this paper, we characterize the much rarer Al-diopside-rich chondrules in QUE 94411/94627 and HH 237, which are texturally and chemically somewhat different from the barred-olivine chondrules.

Two of the Al-diopside-rich chondrules are mineralogically similar to the forsterite-bearing pyroxene-spinel CAIs described above. These chondrules have rounded shapes, compact textures and consist of Al-diopside, forsterite, and minor spinel (Fig. 10). Forsterite occurs as skeletal, elongated inclusions

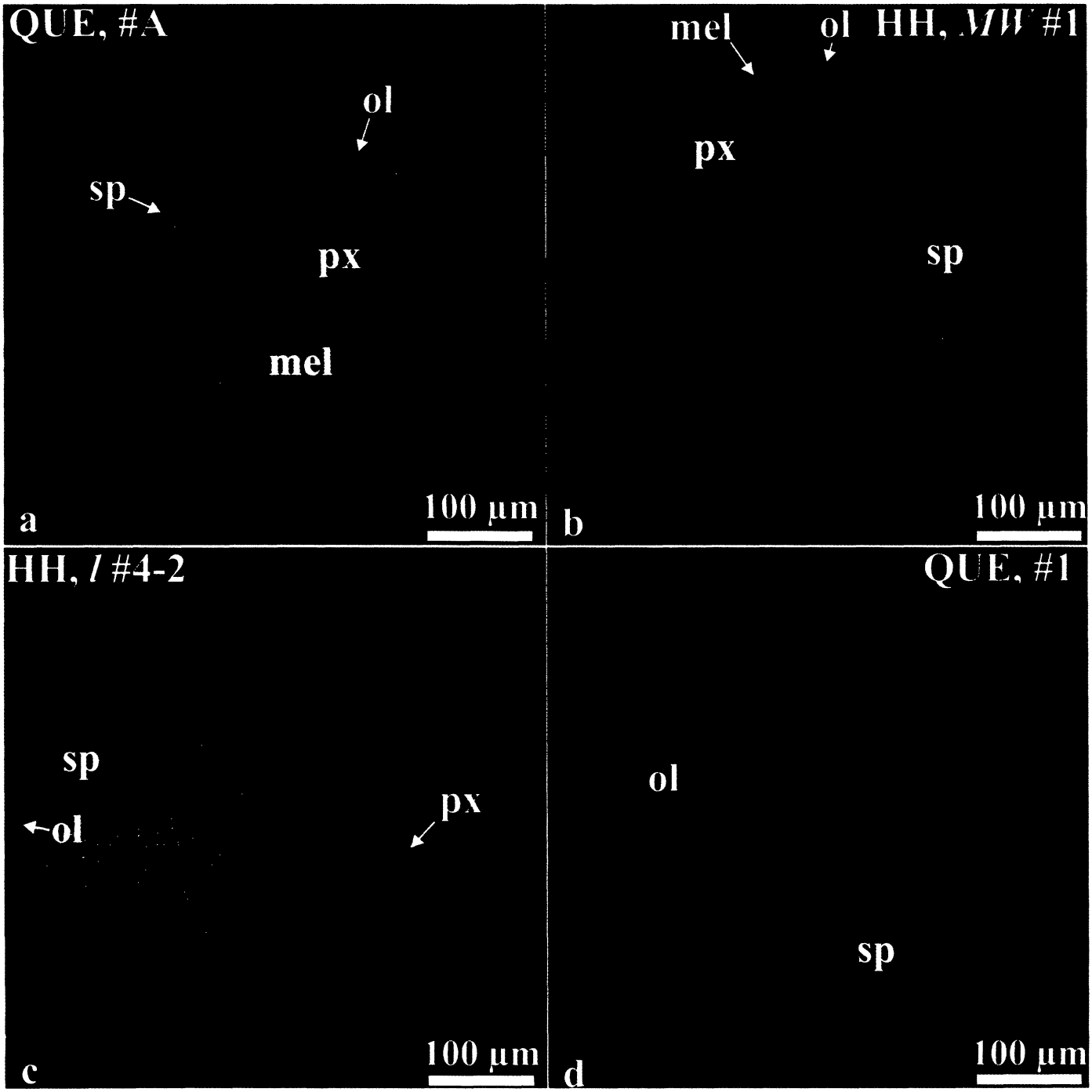

FIG. 5. Combined elemental maps in Mg (red), Ca (green) and Al Kα (blue) x-rays of the pyroxene-spinel ± melilite CAIs from HH 237 and QUE 94411/94627. Modal abundances of pyroxene, spinel, and melilite range broadly. The CAIs are surrounded by forsterite rims of variable thickness.

in Al-diopside and as compact rims around the chondrules; anhedral spinel grains are largely concentrated in the chondrule peripheries.

Three of the Al-diopside-rich chondrules consist of anhedral grains of Al-diopside and interstitial Al-rich, low-Ca pyroxene, and anorthitic mesostasis (Figs. 11 and 12). The Al-diopside grains contain numerous oriented inclusions of forsterite (Fig. 12a); occasionally, forsterite grains occur in interstitial regions together with low-Ca pyroxene (Fig. 12c). The Al-rich, low-Ca pyroxenes contain tiny inclusions of spinel (Fig. 12b). In some cases, spinel is concentrated in the peripheral regions of the Al-diopside grains; the spinel-bearing portions of these grains are depleted in Al relative to the grain cores (Fig. 12d).

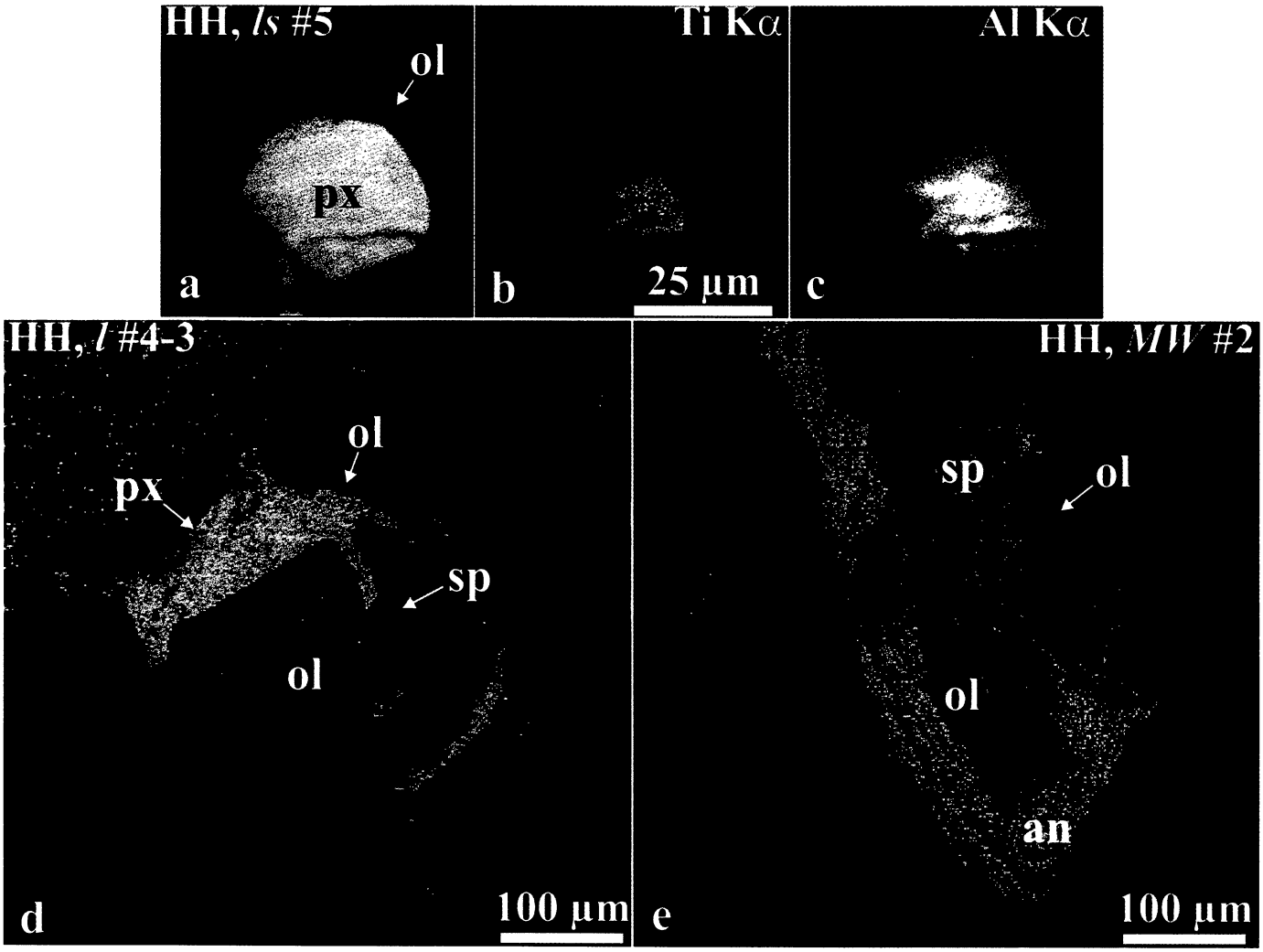

FIG. 6. Combined elemental maps in Mg (red), Ca (green) and Al Kα (blue) x-rays (a, d, e) and x-ray elemental maps in Ti (b) and Al Kα (c) of the pyroxene-rich (a–c) and forsterite-bearing CAIs (d–e) from HH 237. (a–d) Al,Ti-diopside spherule (px) surrounded by a forsterite rim. The pyroxene shows significant compositional variations in Al and Ti. (d) Forsterite-bearing pyroxene-spinel CAI associated with a chondrule-like anorthite-rich material (see also Fig. 7a–d). (e) Forsterite-bearing pyroxene-spinel CAI; forsterite forms inclusions in pyroxene and rims around the CAI.

One of the Al-diopside-rich chondrules is composed of skeletal forsterite crystals overgrown by Al-diopside, and interstitial anorthitic mesostasis (Fig. 13).

Mineral Chemistry

Hibonite in the HH 237 and QUE 94411/94627 CAIs is MgO- and TiO_2-poor (<1.6 wt%). Grossite and perovskite have nearly pure end-member compositions ($CaAl_4O_7$ and $CaTiO_3$, respectively) (Table 2). Plagioclase is nearly pure anorthite, with Na and K contents below the detection limits of EPMA (<0.05–0.04 wt%) (Table 2). Olivine is nearly pure forsterite ($Fa_{<1.5}$), but is enriched in CaO (0.5–1.5 wt%) (Table 2). Olivine grains in the Al-diopside-rich chondrules are too fine grained for quantitative EPMA.

Melilite is compositionally uniform within an individual CAI; however, it shows a large range in åkermanite content between different inclusions ($Åk_{5–78}$) (Table 3). Melilite in the hibonite-melilite-rich and grossite-rich CAIs generally has a lower Åk content (5–17 mol%) than that of the pyroxene-spinel ± melilite CAIs (4–78 mol%). The highest Åk-content ($Åk_{78}$) was found in the forsterite-bearing CAI #1-1 (Fig. 7e).

High-Ca pyroxenes in the CAIs are MnO-, Na_2O- and K_2O-free (<0.07, <0.05, <0.04 wt%, respectively) and Cr_2O_3-poor (<0.15 wt%). These pyroxenes have significant variations in MgO (4–27 wt%), Al_2O_3 (0–26 wt%), and TiO_2 (0–17 wt%) contents within individual inclusions and between different CAIs (Table 4, Fig. 14). High-Ti Al-diopsides (fassaite) are rare and occur in cores of some pyroxene-spinel ± melilite CAIs; rim pyroxenes have always low concentrations of Al_2O_3 and TiO_2 (Table 4).

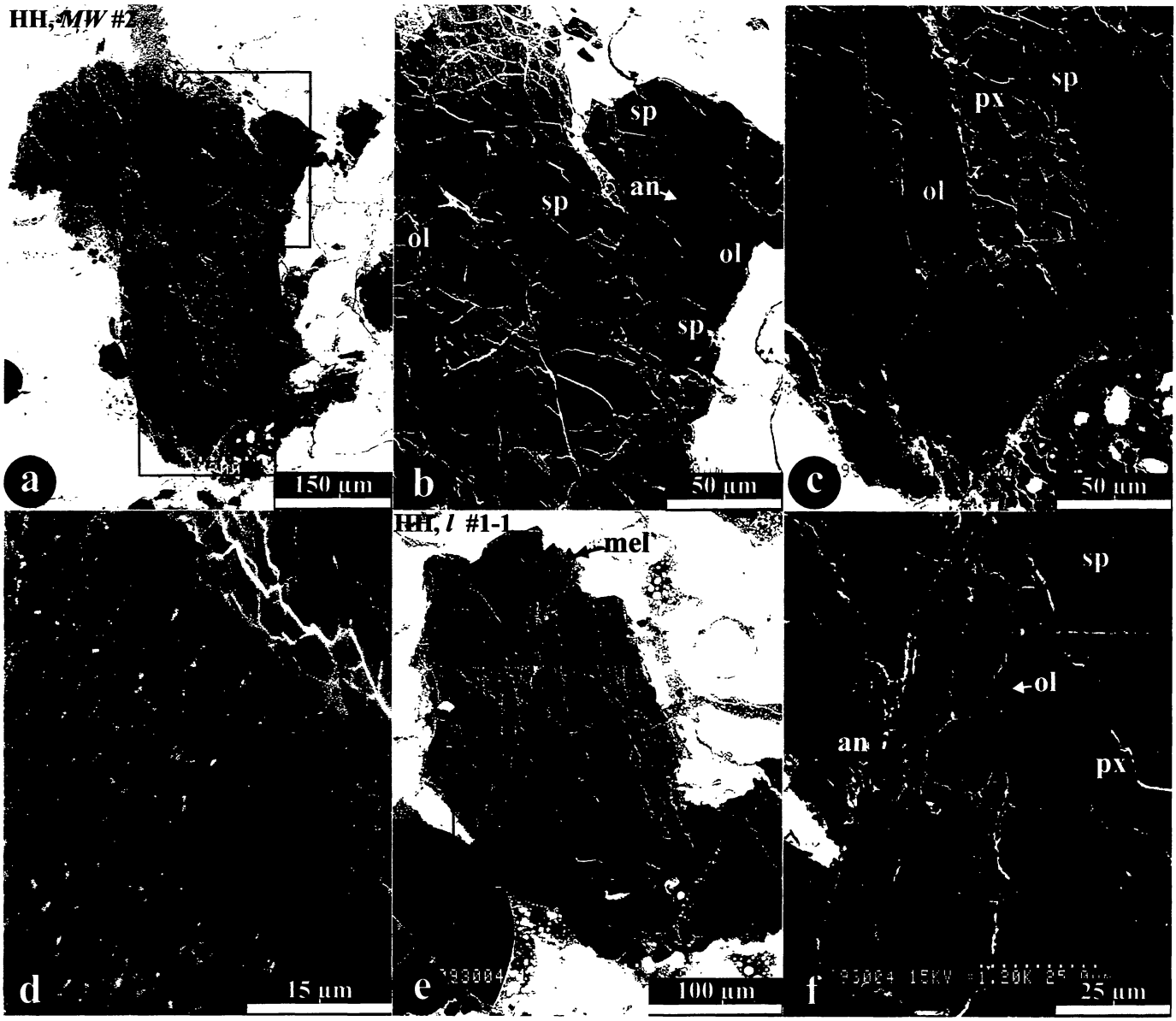

FIG. 7. Backscattered electron images of the forsterite-bearing refractory inclusions from HH 237. (a–d) Forsterite-bearing pyroxene-spinel CAI associated with a chondrule-like anorthite-rich material; the latter consists of anorthite, high-Ca pyroxene and silica-rich mesostasis (mes). Regions outlined in (a) are shown in detail in (b) and (c). (e, f) Forsterite-bearing pyroxene-melilite-spinel-anorthite CAI. Region outlined in (e) is shown in detail in (f).

High-Ca pyroxenes of the Al-diopside-rich chondrules are compositionally similar to those of the pyroxene-spinel ± melilite CAIs, but occasionally have higher abundances of Cr_2O_3 (up to 1.1 wt%) (Table 5, Fig. 14). Low-Ca pyroxenes are characterized by high concentrations of Al_2O_3 (9–14 wt%) and commonly show significant deviations from stoichiometry, possibly due to tiny inclusions of spinel and/or anorthitic glass (Table 5).

Spinel of the CB CAIs is poor in FeO (<1.2 wt%), Cr_2O_3 (0.1–0.6 wt%), and V_2O_3 (<0.8 wt%) (Table 6). Spinel grains in the Al-diopside-rich chondrules are too fine grained for quantitative EPMA.

Bulk Compositions of Calcium-Aluminum-Rich Inclusions and Chondrules: Major Elements

Bulk major element compositions of the CAIs and chondrules in HH 237 and QUE 94411/94627 are listed in Tables 7 and 8 and shown in Figs. 15 and 16. They are less refractory on average than those in CH chondrites, which are characterized by high abundance of hibonite and grossite (Weber *et al.*, 1995). They are similar to the CR CAIs (Weber and Bischoff, 1997), but generally do not contain anorthite. The Al-diopside-rich chondrules are compositionally similar to the most Al-rich barred-olivine chondrules, but generally

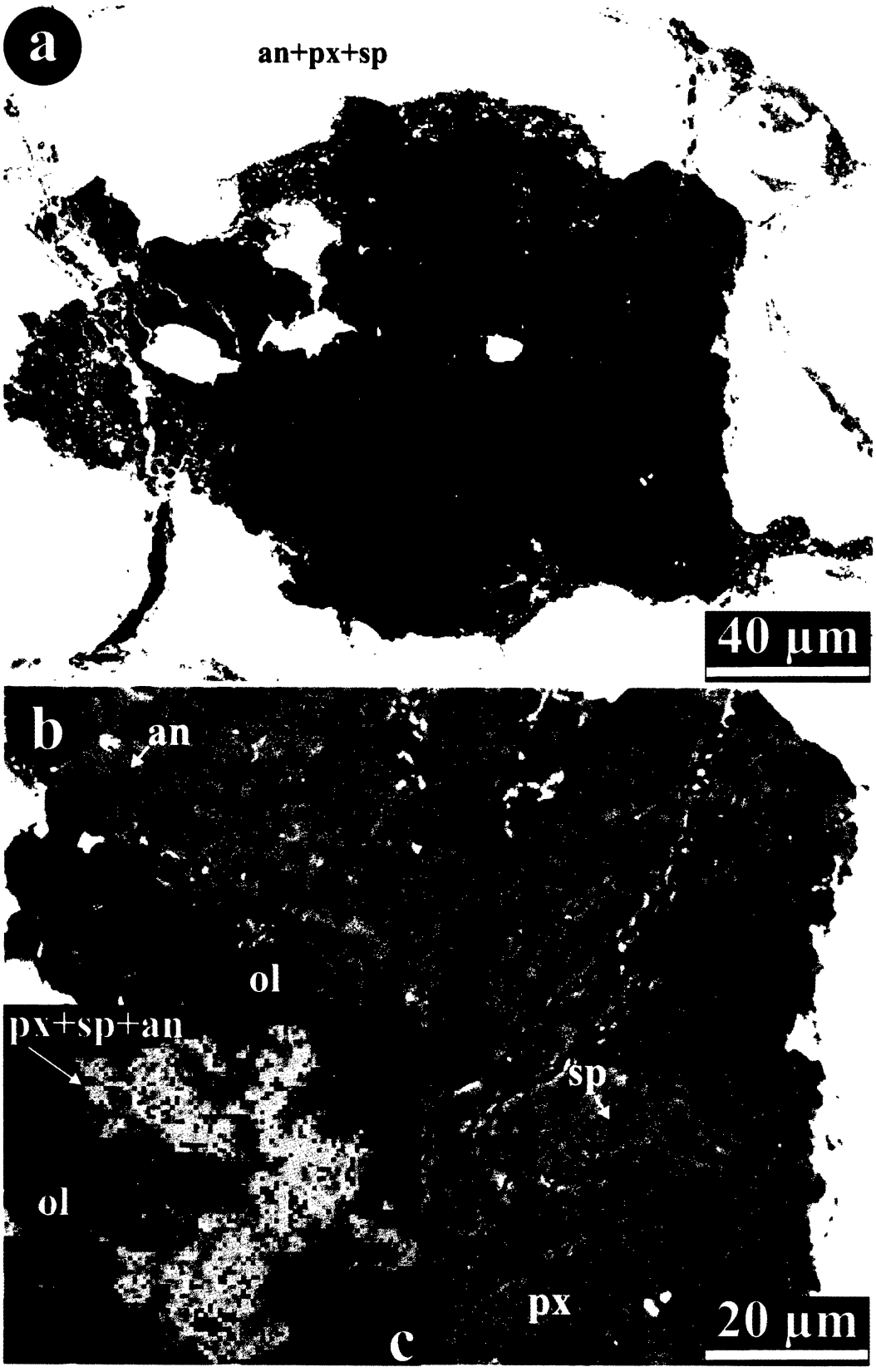

FIG. 8. Backscattered electron images and combined elemental map in Mg (red), Ca (green) and Al Kα (blue) x-rays of an amoeboid olivine aggregate #1-3 from HH 237. The aggregate consists of fine-grained pyroxene-spinel-anorthite material surrounded by a thick forsterite mantle containing large nodules of FeNi-metal.

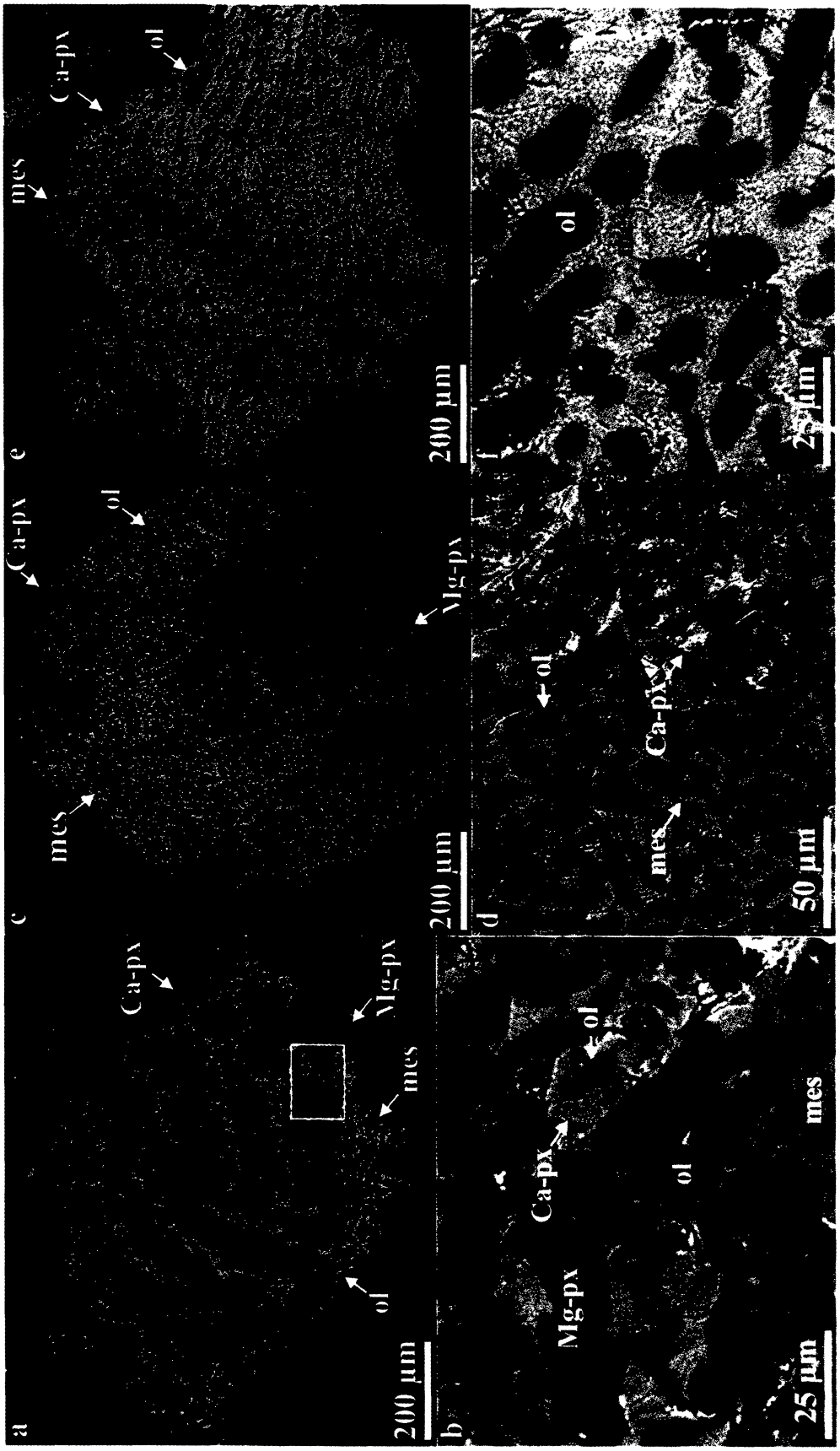

FIG. 9. Combined elemental maps in Mg (red), Ca (green) and Al Kα (blue) x-rays (a, c, e) and BSE images (b, d, f) of barred-olivine chondrules from HH 237. The chondrules consist of variable amounts of forsterite, Al-rich high-Ca pyroxene (Ca-px), Al-rich low-Ca pyroxene (Mg-px), and anorthitic mesostasis.

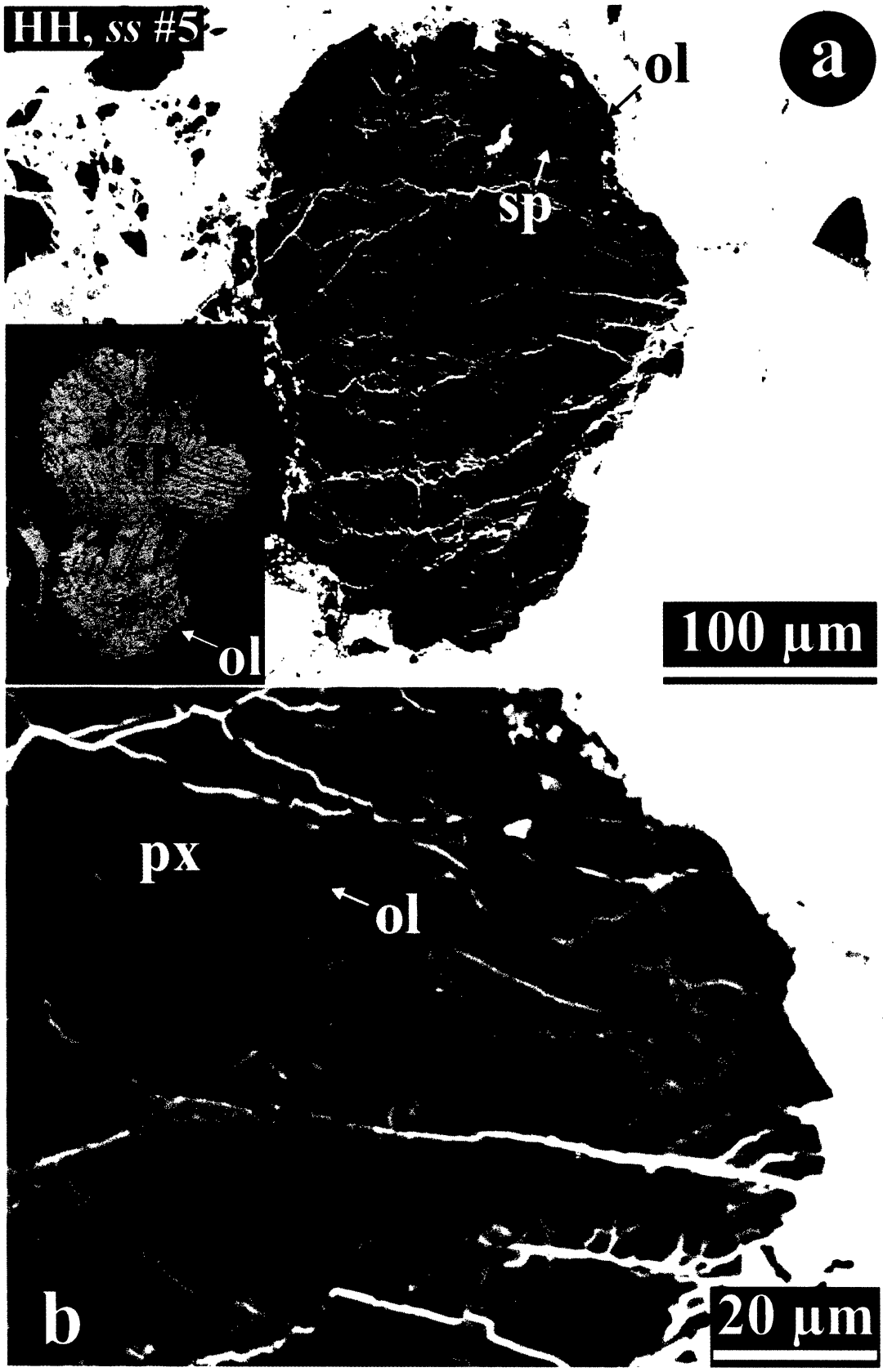

FIG. 10. Backscattered electron images and combined elemental map in Mg (red), Ca (green) and Al Kα (blue) x-rays of an Al-diopside-rich chondrule #5 from HH 237. The chondrule consists of Al,Ti-diopside (px) with numerous inclusions of forsterite; spinel is minor. It is surrounded by a forsterite rim.

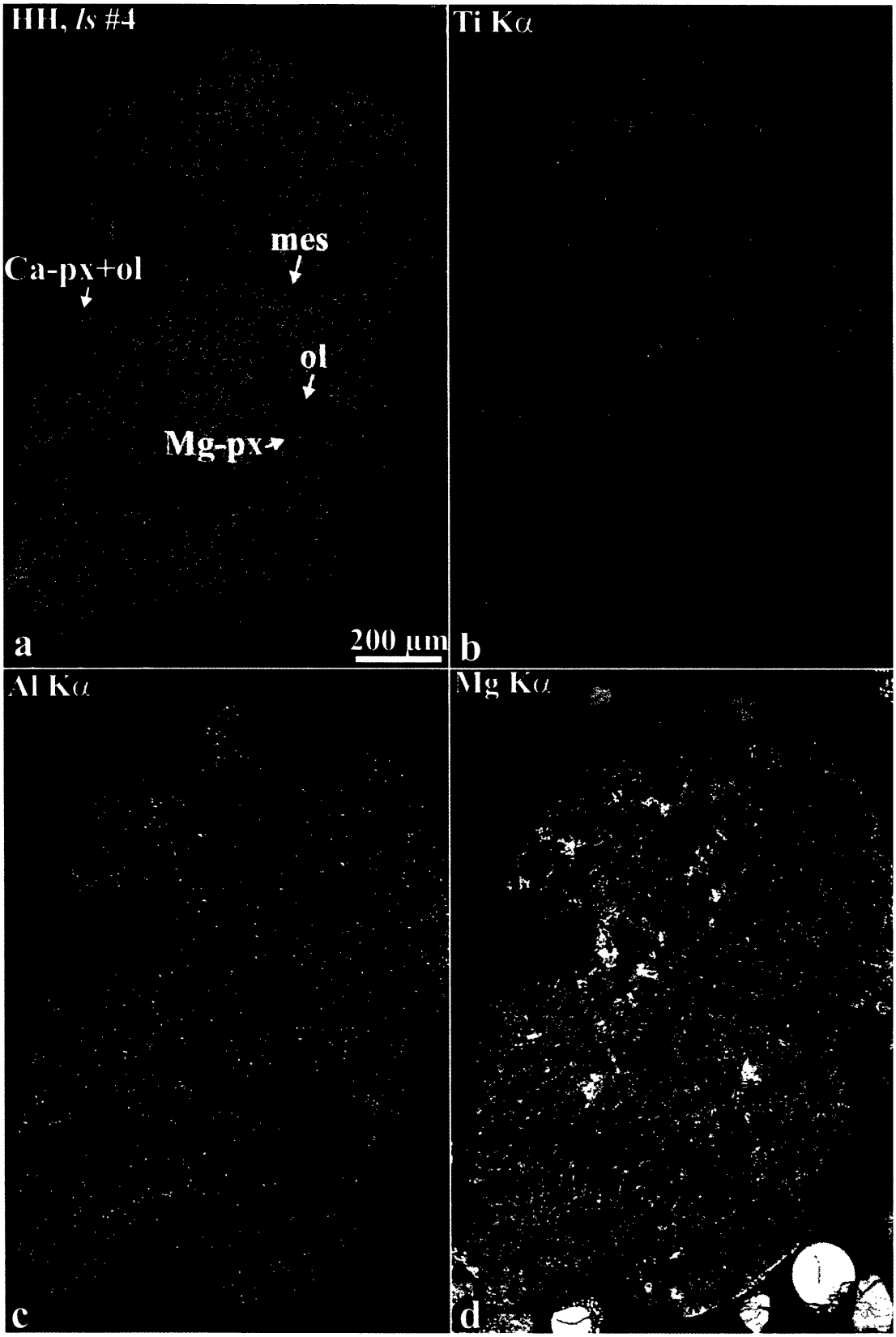

FIG. 11. Combined elemental map in Mg (red), Ca (green) and Al Kα (blue) x-rays (a) and x-ray elemental maps in Ti (b), Al (c) and Mg Kα (d) of an Al-diopside-rich chondrule #4 from HH 237 (see also Fig. 12). The chondrule contains Al-diopside (Ca-px) with numerous inclusions of forsterite, and interstitial material composed of Al-rich, low-Ca pyroxene (Mg-px), forsterite, and anorthitic mesostasis (mes). The low-Ca pyroxenes contain tiny inclusions of spinel.

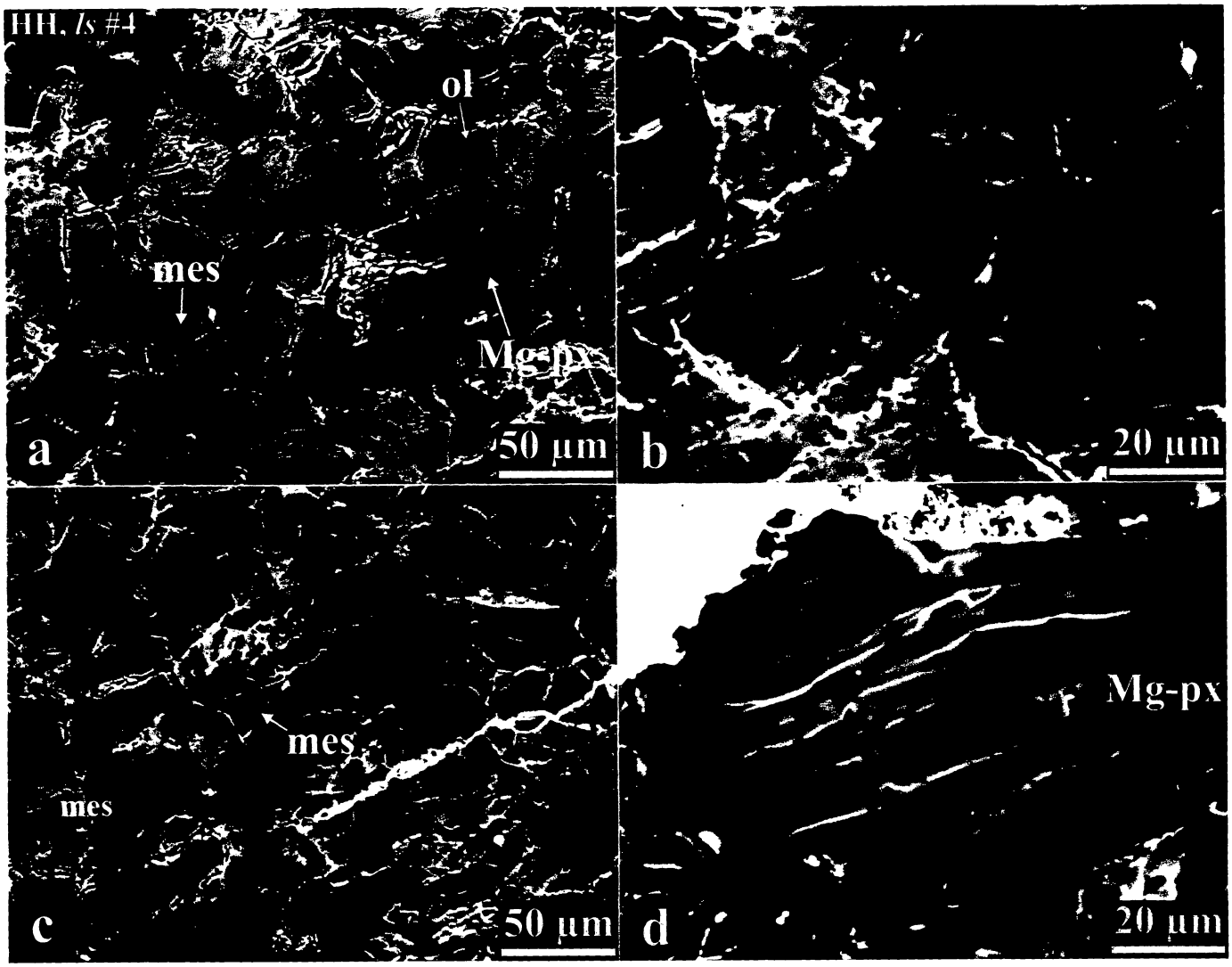

FIG. 12. Backscattered electron images of the Al-diopside-rich chondrule shown in Fig. 11. (a, b) Chondrule consists of Al-diopside with numerous forsterite inclusions, Al-rich, low-Ca pyroxene with small spinel inclusions, and anorthitic mesostasis. (c) Forsterite grains occupy interstitial regions between the Al-diopside grains. (d) Spinel grains overgrowing Al-diopside.

have lower Cr concentrations; cryptocrystalline chondrules are less refractory than barred-olivine and Al-diopside-rich chondrules.

Bulk Compositions of Calcium-Aluminum-Rich Inclusions and Chondrules: Rare Earth Element Abundances

Bulk rare earth element (REE) concentrations in CAIs and chondrules (barred-olivine and cryptocrystalline) are listed in Table 9; REE abundance patterns normalized to CI are shown in Fig. 17. None of the chondrules analyzed, however, belong to the category of Al-diopside-rich chondrules described above. Barred-olivine and cryptocrystalline chondrules have unfractionated REE patterns that range from ~10× CI to <0.01× CI; barred-olivine chondrules have higher REE abundances than cryptocrystalline chondrules.

In the hibonite-melilite CAI #4-1 (Fig. 2a), REE abundances are enriched by a factor of ~100 over CI. The abundance pattern exhibits negative anomalies in Ce, Eu and Yb. Two of the CAIs, #4-2 and #1-1, largely composed of Al-diopside, spinel, and minor melilite (Figs. 4d and 6i) have flat (group I) REE patterns at ~10 × CI, except for a negative Eu anomaly (Fig. 17).

Oxygen-Isotopic Compositions

Oxygen-isotopic compositions of primary minerals in eight CAIs, two Al-diopside-rich chondrules, and one cryptocrystalline chondrule are listed in Table 10 and shown in Fig. 18. All mineralogical types of the CAIs described above

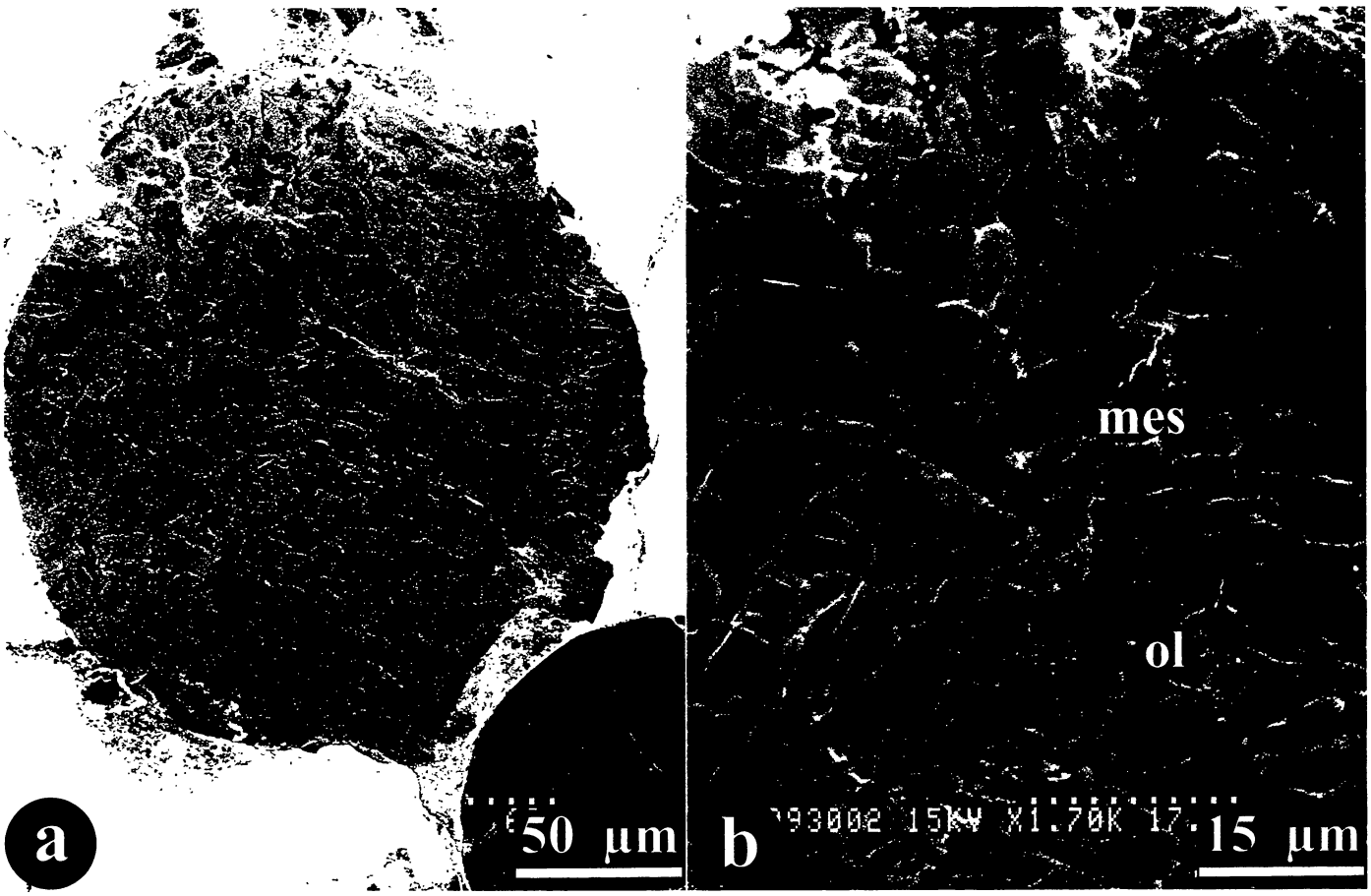

FIG. 13. Backscattered electron images of Al-diopside-rich chondrule #5a from HH 237. The chondrule consists of skeletal forsterite grains overgrown by Al-diopside, and interstitial anorthitic mesostasis.

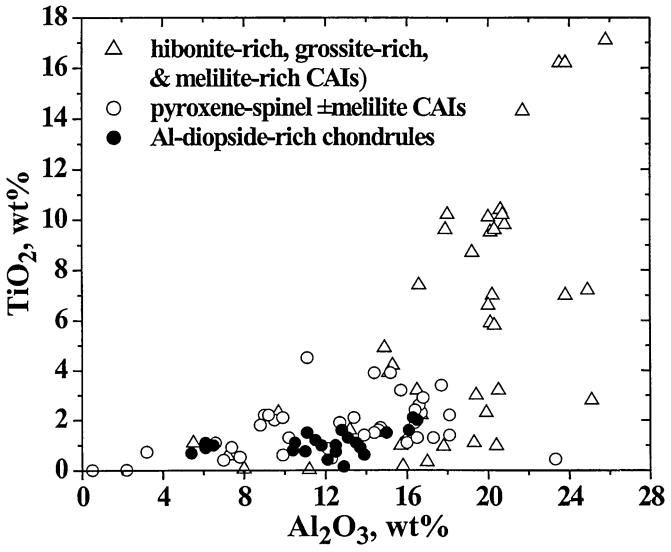

FIG. 14. Concentrations of Al_2O_3 *vs.* TiO_2 in high-Ca pyroxenes in the CAIs and Al-diopside-rich chondrules from HH 237 and QUE 94411/94627.

have relatively heavy O-isotopic compositions with $\Delta^{17}O$ ranging from –6‰ to –10‰ ($1\sigma \approx 1.3$‰). Variations in O-isotopic compositions of different minerals within an individual CAI are small. Two Al-diopside-rich chondrules analyzed have similar O-isotopic compositions ($\Delta^{17}O \approx -7 \pm 1.1$‰) to those of CAIs. A Ca,Al-poor cryptocrystalline chondrule from QUE 94411/94627 has heavier O-isotopic composition than CAIs and Al-diopside-rich chondrules ($\Delta^{17}O \approx -3 \pm 1.4$‰).

DISCUSSION

Comparison of Calcium-Aluminum-Rich Inclusions in Hammadah al Hamra 237 and Queen Alexandra Range 94411/94627 to Those in Other Chondrite Groups

A comparison between CAIs in HH 237 and QUE 94411/94627 and those in other chondrite groups shows that all CAI types exist in at least one of the carbonaceous chondrite groups (Table 11). Alteration minerals, such as secondary nepheline and sodalite, which are common in CAIs from the CO, oxidized CV and ordinary chondrites (Bischoff and Keil, 1984; MacPherson *et al.*, 1988; Russell *et al.*, 1998), are absent in the refractory inclusions from HH 237 and QUE 94411/94627.

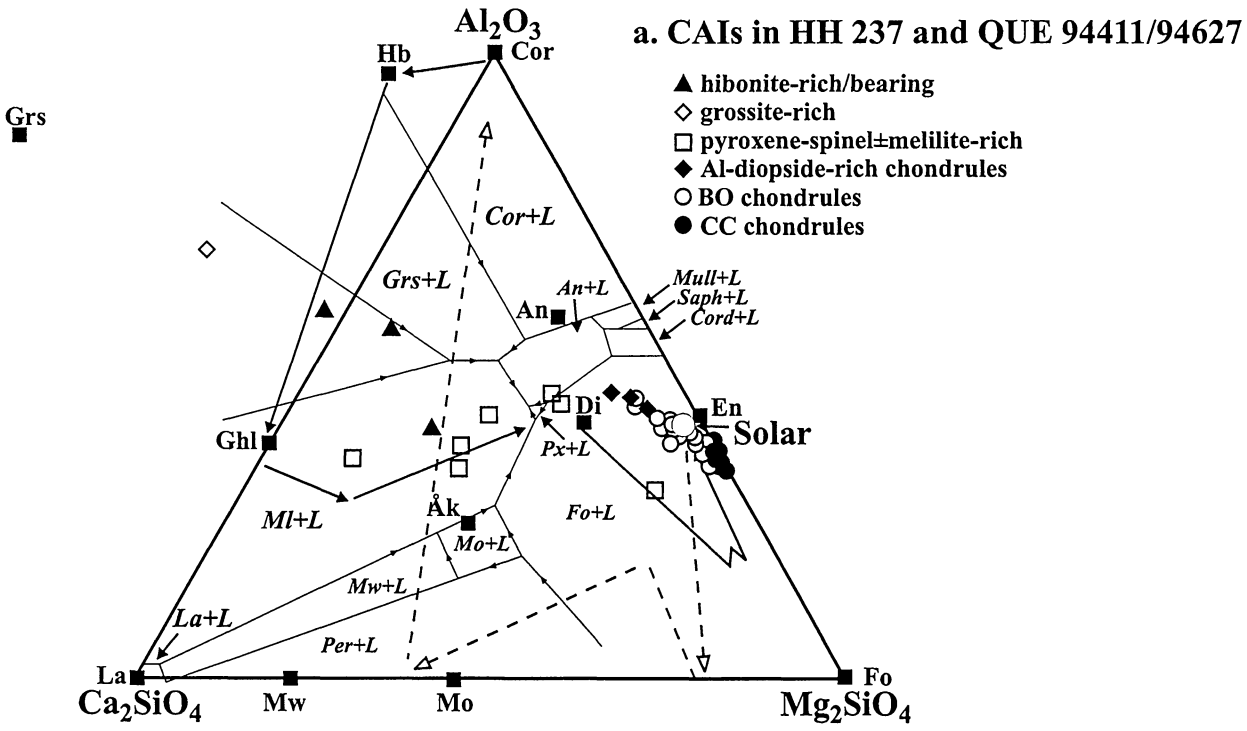

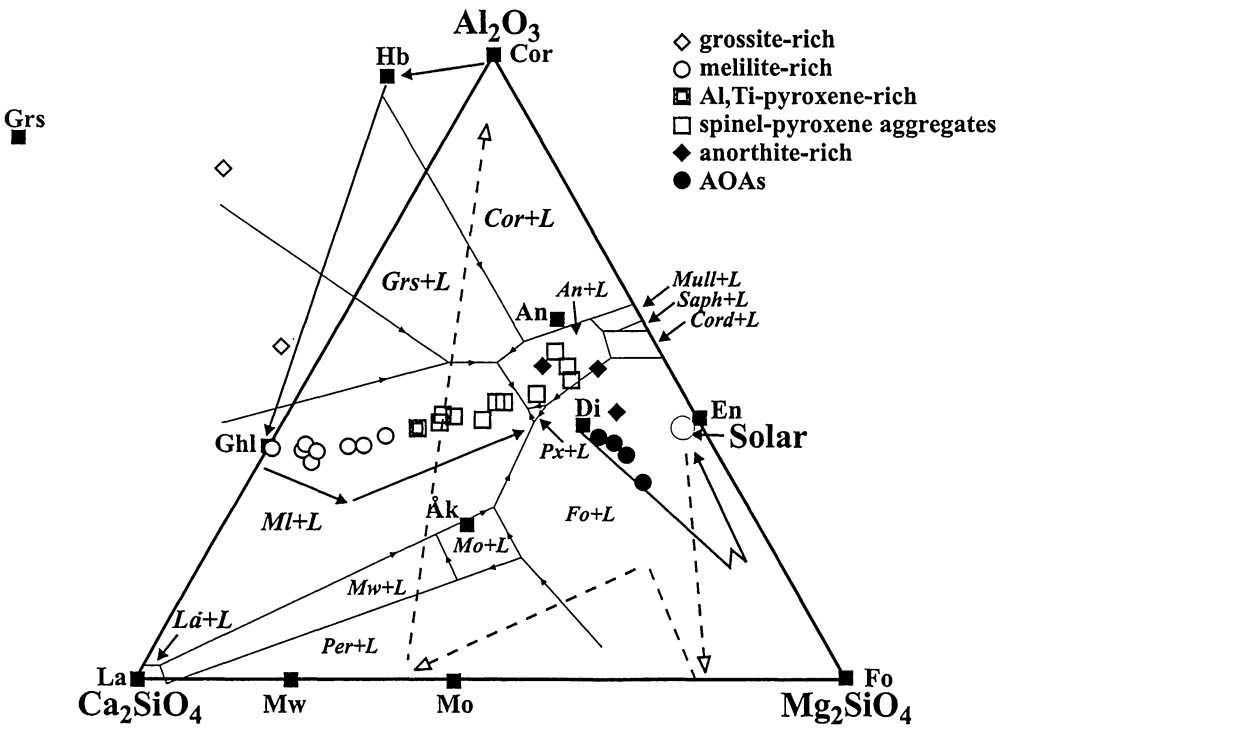

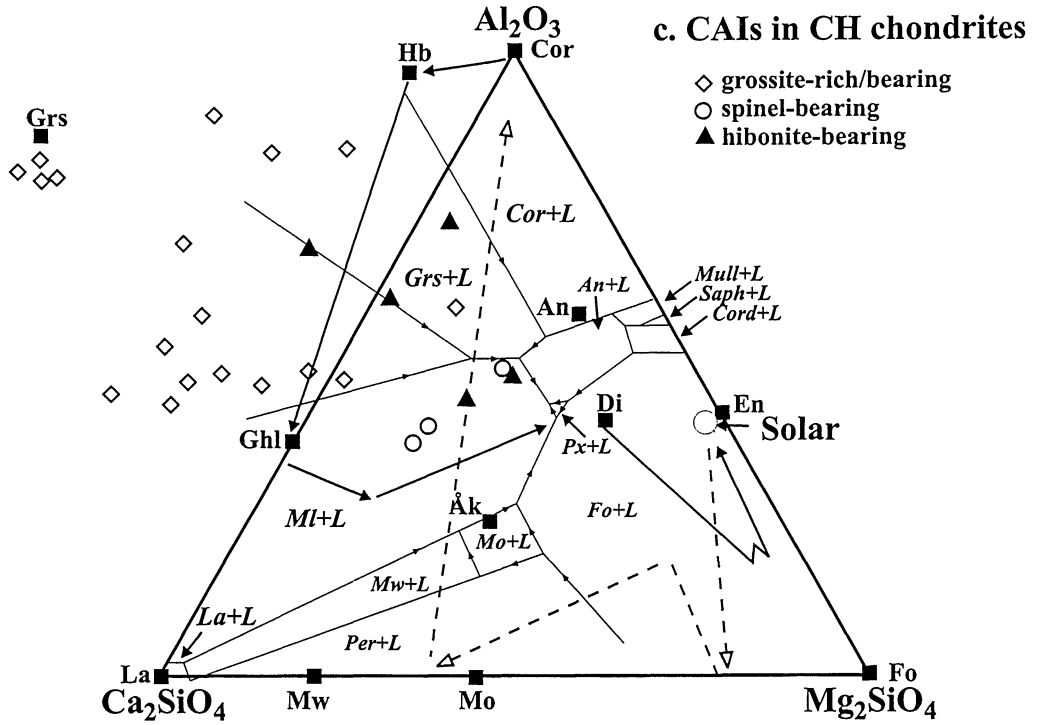

FIG. 15. *(left and above)* Bulk compositions of CAIs and Al-diopside-rich, barred-olivine and cryptocrystalline chondrules from the HH 237 and QUE 94411/94627 (a), CR (b) and CH (c) carbonaceous chondrites, projected from spinel onto the plane larnite (La) – forsterite (Fo) – corundum (Cor), together with the spinel-saturated liquidus relationships in this system; solid vectors show calculated trajectory for bulk condensed solids during equilibrium condensation; dashed vectors show experimentally-determined compositions of liquids during melt evaporation (after MacPherson and Huss, 2000). CAIs in the HH 237, QUE 94411/94627 and CR CAIs are less refractory on average than those in CH chondrites and roughly follow equilibrium condensation path. The Al-diopside-rich chondrules are compositionally similar to the most Al-rich barred-olivine chondrules. Bulk compositional data of the CR and CH CAIs are from Weber and Bischoff (1997) and Weber and Bischoff (1994), respectively.

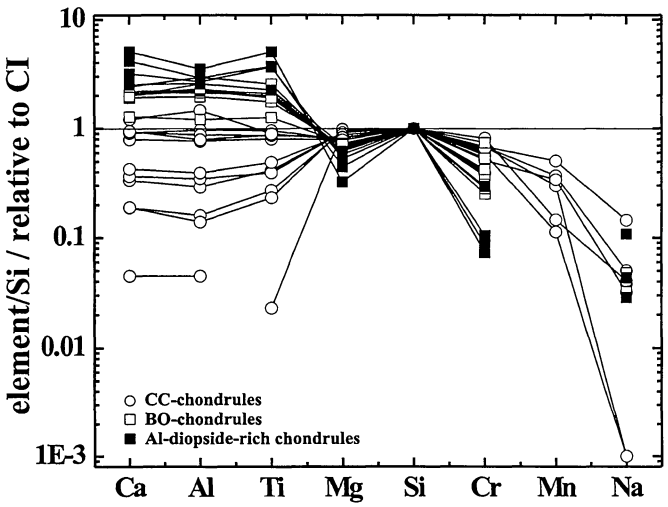

FIG. 16. Bulk contents of lithophile elements normalized to Mg and CI chondrite abundances in barred-olivine, cryptocrystalline and Al-diopside-rich chondrules in HH 237 and QUE 94411/94627. The Al-diopside-rich chondrules are compositionally similar to the most Al-rich barred-olivine chondrules; the former are slightly depleted in Cr, however.

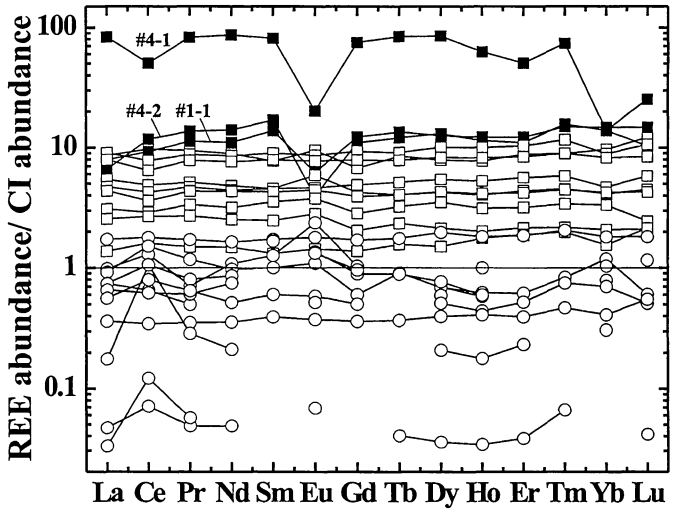

FIG. 17. Rare earth element patterns in the CAIs (solid squares), barred-olivine (open squares) and cryptocrystalline chondrules (open circles) in HH 237 and QUE 94411/94627.

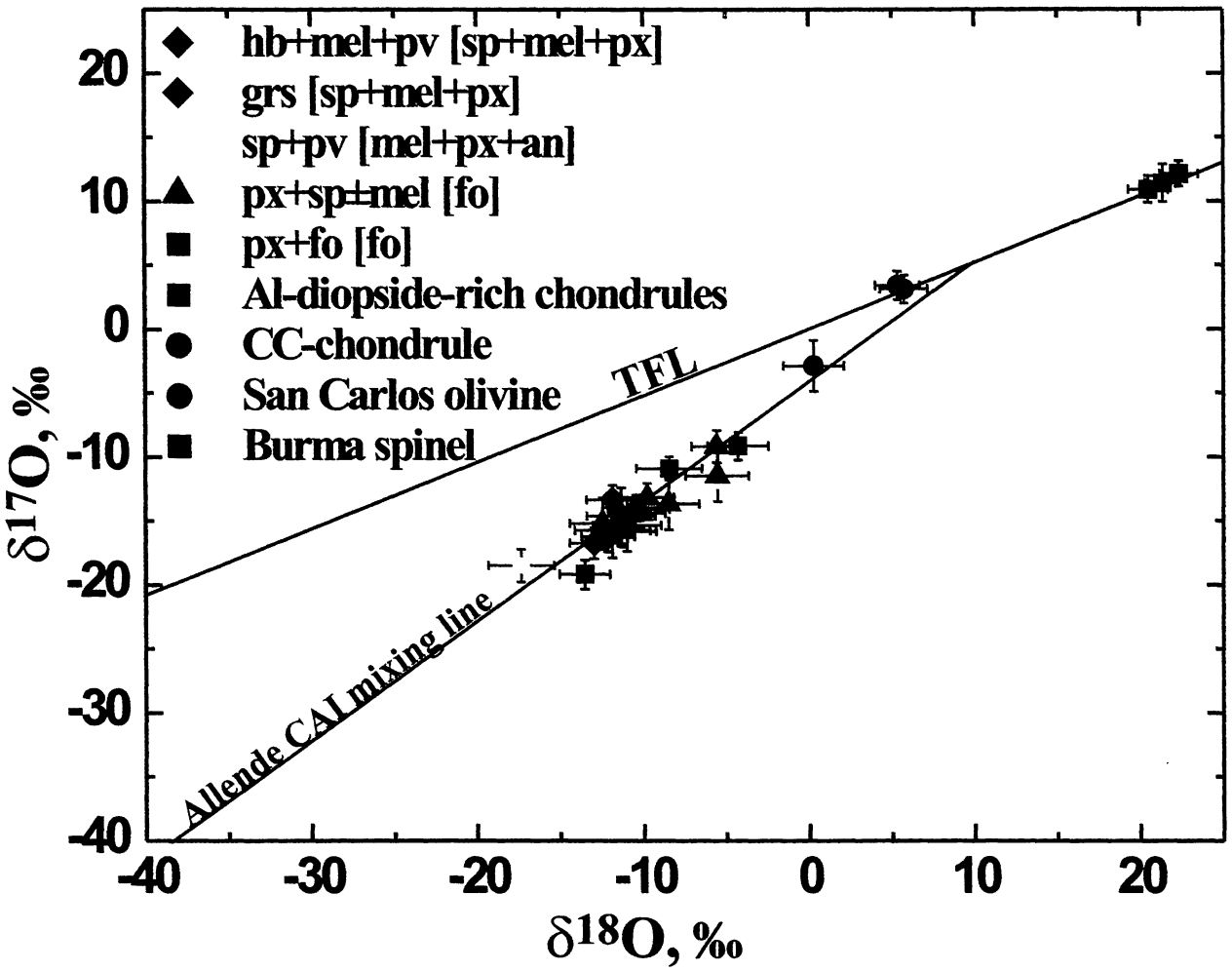

FIG. 18. Oxygen-isotopic compositions of CAIs, Al-diopside-rich and cryptocrystalline chondrules in HH 237 and QUE 94411/94627.

Similar to CAIs in CO, CM and two ungrouped chondrites MacAlpine Hills (MAC) 88107 and MAC 87300, the most abundant (56%) CAIs in HH 237 and QUE 94411/94627 are pyroxene-spinel-rich inclusions (MacPherson *et al.*, 1983, 1984; Greenwood *et al.*, 1992, 1994; Russell *et al.*, 1998, 2000a). However, there are mineralogical and textural differences between the pyroxene-spinel-rich inclusions in HH 237 and QUE 94411/94627 and other chondrite groups. Melilite is rare in the pyroxene-spinel-rich CAIs in CM chondrites, but it is a common mineral in those in HH 237, QUE 94411/94627, CO, CR, MAC 87300, and MAC 88107. In these meteorites, there is a continuum between the pyroxene-rich and melilite-rich CAIs (Figs. 2c and 5).

The pyroxene-spinel-rich inclusions in CO, CR, MAC 87300 and MAC 88107 occur as irregularly-shaped objects composed of nodules, chains, or bands of spinel that are rimmed by pyroxene and phyllosilicates, commonly with minor perovskite, melilite, or hibonite (MacPherson *et al.*, 1983, 1984; Greenwood *et al.*, 1992, 1994; Russell *et al.*, 1998, 2000a; Weisberg and Prinz, 1990; Weber and Bischoff, 1997). These CAIs are texturally and mineralogically similar to a spinel-rich inclusion #C in QUE 94411/94627 (Fig. 3e,f). The pyroxene-spinel ± melilite inclusions in HH 237 and QUE 94411/94627 have compact textures and consist of euhedral to subhedral grains of spinel embedded in Al-diopside and melilite, suggesting an igneous origin. Considering the mineralogy, textures, and chemical composition (presence of Ti^{3+} in pyroxene), some of the pyroxene-spinel ± melilite CAIs resemble type B CAIs in CV chondrites (Grossman, 1980). The HH 237 and QUE 94411/94627 CAIs, however, are typically rimmed by forsterite. Similar forsterite rims were described around pyroxene-spinel spherules in CH chondrites (Krot *et al.*, 1999). Forsterite has also been observed as a minor component of Wark–Lovering rims around CAIs in CV, CR, MAC 88107 and MAC 87300 (MacPherson *et al.*, 1988; Russell *et al.*, 2000a; Krot, unpubl. data) and as thick mantles around some CAIs from CM and CV chondrites (MacPherson *et al.*, 1984, 1988).

Forsterite-bearing CAIs, previously described only in CV chondrites (Blander and Fuchs, 1975; Dominik *et al.*, 1978; Wark *et al.*, 1987; Clayton *et al.*, 1977, 1984; Davis *et al.*, 1991, 2000; Krot *et al.*, 2000b), are rather common (~28%) in HH 237 and QUE 94411/94627. However, the forsterite-bearing CAIs in HH

TABLE 11. Types of refractory inclusions associated with chondrite groups.

CAI type	HH 237/QUE	CV	CO	CM	CK	OC	EC	CH	CR
Melilite-rich (type A)	rare	common	common	rare	–	rare	–	common	common
Al,Ti-px-rich (type B)	rare	common	–	–	rare	–	–	–	rare
Amoeboid olivine aggregates	rare	common	common	common	common	–	–	–	common
Forsterite-bearing	rare	rare	–	–	–	–	–	–	–
Spinel ± pyroxene ± melilite-rich	common	common	common	common	rare	rare	rare	common	common
Hibonite ± spinel-rich	rare	common	common	common	–	rare	rare	common	rare
Grossite-rich	rare	–	rare	–	–	–	–	common	rare
Ca-pyroxene spherules	rare	–	rare	rare	–	–	rare	common	–

Modified from MacPherson *et al.* (1988). Additional data: CH chondrites, Weber and Bischoff (1994), Kimura *et al.* (1993); CO chondrites, Greenwood *et al.* (1992), Russell *et al.* (1998); CM chondrites, MacPherson *et al.* (1983, 1984), Simon *et al.* (1994); CR chondrites, Weisberg and Prinz (1990), Weisberg *et al.* (1993), Kallemeyn *et al.* (1994); Weber and Bischoff (1997); CK chondrites, McSween (1977), MacPherson and Delaney (1985), Kallemeyn *et al.* (1991), Keller *et al.* (1992), Noguchi (1993); EC chondrites, Bischoff *et al.* (1985), Guan *et al.* (1999), Fagan *et al.* (2000); QUE/HH 237, this study.

237 and QUE 94411/94627 are mineralogically and texturally different from those in CV chondrites. The latter are larger, enriched in melilite, and surrounded by well-developed Wark–Lovering rims which have up to five mineralogically different layers instead of one or two in the CAIs studied here.

Similar to most chondrite groups, but in contrast to CH chondrites, grossite-rich and hibonite-rich CAIs are rare in HH 237 and QUE 94411/94627 (MacPherson *et al.*, 1989; Kimura *et al.*, 1993; Weber and Bischoff, 1994, 1997; Krot *et al.*, 1999). The hibonite-rich CAIs in HH 237 an QUE 94411/94627 with lath-shaped hibonite and interstitial melilite and perovskite are similar to the hibonite-perovskite-spinel-melilite CAI 1805-1 in Semarkona (Bischoff and Keil, 1984; Fig. 10.3.17 in MacPherson *et al.*, 1988), although the rim mineralogy is different. The grossite-rich CAI and one of the hibonite-rich CAIs in HH 237 are surrounded by melilite-Al-diopside rims, like many CAIs in CH chondrites (Weber and Bischoff, 1992, 1994; Krot *et al.*, 1999).

Similar to CH chondrites, but in contrast to other carbonaceous chondrite groups, AOAs are rare in HH 237 and QUE 94411/94627 (MacPherson *et al.*, 1989; Kimura *et al.*, 1993).

To summarize, CAIs in the metal-rich chondrites HH 237 and QUE 94411/94627, as a group of objects, are texturally, mineralogically, and isotopically different from CAIs in other chondrite groups. (1) They are dominated by rounded, compact-type pyroxene-spinel ± melilite and forsterite-bearing, pyroxene-spinel ± melilite inclusions. (2) Most of the CAIs in HH 237 and QUE 94411/94627 are surrounded by forsterite rims. (3) The majority of CAIs in other chondrite groups are characterized by ^{16}O-rich isotopic compositions ($\Delta^{17}O < -20‰$), with spinel, pyroxene, grossite, and hibonite enriched and melilite and anorthite depleted in ^{16}O within an individual CAI (Clayton *et al.*, 1973, 1977; McKeegan *et al.*, 1998b). In contrast, the CAIs studied here have ^{16}O-poor oxygen isotopes with $\Delta^{17}O$ ranging from –6‰ to –10‰ for all analyzed CAI minerals (grossite, hibonite, melilite, pyroxene, spinel). This suggests that the CAIs in HH 237 and QUE 94411/94627 formed in a reservoir isotopically distinct from the reservoir(s) where usual, ^{16}O-rich ($\Delta^{17}O < -20‰$) CAIs in other chondritic meteorites formed.

Arguments Against an Impact Origin of the Metal-Rich Chondrites: Evidence from Calcium-Aluminum-Rich Inclusions

Wasson and Kallemeyn (1990) and Wasson (2000, pers. comm.) argued that cryptocrystalline and barred-olivine chondrules, dominant in the HH 237, QUE 94411/94627, and CH chondrites, resulted from melting, vaporization, outgassing, and condensation in a cloud of impact ejecta on the CR parent asteroid. According to this hypothesis, rare CAIs in the HH 237, QUE 94411/94627, and CH chondrites either survived this impact event or were added later, during regolith gardening together with typical ferromagnesian chondrules of porphyritic textures (type I and type II). The observed differences in textures and mineralogy of CAIs in the HH 237, QUE 94411/94627, CH, and CR chondrites exclude the origin of these inclusions and their host meteorites from CR chondritic material, only. In addition, because both HH 237 and QUE 94411/94627 lack chondrules of porphyritic textures, addition of CAIs with "normal" chondritic materials during regolith gardening can be excluded. Therefore, it seems unlikely that the metal-rich chondrites formed by impact processing of the CR asteroidal body.

Crystallization History of Calcium-Aluminum-Rich Inclusions in Hammadah al Hamra 237 and Queen Alexandra Range 94411/94627

The compact textures of most CAIs studied here suggest that they probably crystallized from melts. The crystallization history of the CAIs can be inferred from their estimated bulk compositions, petrographic observations and crystallization experiments on melts of similar compositions (*e.g.*, Stolper, 1982; Beckett and Stolper, 1994).

The dominant pyroxene-spinel ± melilite CAIs in HH 237 and QUE 94411/94627 are characterized by compact textures with euhedral-to-subhedral spinel grains embedded in Al-diopside and/or melilite; the CAIs are typically surrounded by forsterite rims. Textural relationships between these minerals suggest early crystallization of the spinel-melilite-pyroxene core followed by forsterite. Bulk compositions of most of these CAIs projected from spinel onto the plane larnite-forsterite-corundum plot in the liquidus field of melilite (Fig. 15). (Due to the presence of thick forsterite rims around the spinel-pyroxene CAIs QUE 94411/94627 #1 (Fig. 5d) and HH 237, ls #7, their bulk compositions plot in the liquidus field of forsterite (Fig. 15).) The equilibrium crystallization sequence of melts of such compositions is spinel or melilite → anorthite → pyroxene (Stolper, 1982). Fractional crystallization may result in early appearance of pyroxene, in the crystallization sequence, prior to anorthite. The absence of anorthite in most CAIs in HH 237 and QUE 94411/94627 may reflect difficulty of nucleating anorthite or rapid cooling of the CAI melts (Stolper, 1982).

The presence of forsterite rims around pyroxene-spinel-melilite CAIs, which is not predicted to be a product of an equilibrium crystallization sequence from melts of these compositions (Stolper, 1982), is puzzling. It may suggest that the forsterite rims did not crystallize from the CAI melts, but accreted or condensed later around already solidified CAIs. This interpretation is supported by the presence of forsterite as the outermost layer of a Wark–Lovering rim sequence around hibonite-melilite CAI (Fig. 2a) (Wark–Lovering rims are generally considered to be products of gas-solid reactions between solid CAI and nebula gas; MacPherson *et al.*, 1988).

In contrast to the rim forsterite, some pyroxene-spinel CAIs contain forsterite in their cores; the latter probably crystallized from CAI melts (Fig. 6e–n). This interpretation is consistent with their bulk compositions plotting in the liquidus field of forsterite (Fig. 14).

Bulk compositions of the compact hibonite-melilite CAIs plot near the hibonite-melilite cotectic supporting nearly simultaneous crystallization of these minerals (Beckett and Stolper, 1994).

Comparison of Aluminum-Diopside-Rich Chondrules in Hammadah al Hamra 237 and Queen Alexandra Range 94411/94627 to Aluminum-Rich Chondrules in Other Chondrite Groups

The rare Al-diopside-rich chondrules in HH 237 and QUE 94411/94627 (Figs. 10–13) are mineralogically very similar to rare Al-diopside-rich chondrules in CH chondrites (Krot *et al.*, 1999; unpubl. data). Based on the bulk compositions, the Al-diopside-rich chondrules can be classified as Al-rich chondrules (Bischoff and Keil, 1984). Our mineralogical observations of the Al-rich chondrules in CO, CK, CV, CR, enstatite and ordinary chondrites (Fagan *et al.*, 2000; Krot, 2000) and literature survey show, however, that Al-rich chondrules texturally and mineralogically similar to Al-diopside-rich chondrules are not found in other chondrite groups.

Origin of Aluminum-Diopside-Rich Chondrules: Possible Link between Calcium-Aluminum-Rich Inclusions and Chondrules in Hammadah al Hamra 237 and Queen Alexandra Range 94411/94627

It was recently concluded that chondrules and FeNi-metal grains in HH 237 and QUE 94411/94627 formed by condensation in a solar nebula region with an initially high dust/gas ratio (10–50× solar) that experienced complete vaporization and were subsequently isolated from this region at high ambient temperatures (Meibom *et al.*, 2000; Herzog *et al.*, 2000; Krot *et al.*, 2001; Petaev *et al.*, 2001; Campbell *et al.*, 2001).

Barred-olivine and cryptocrystalline chondrules in HH 237 and QUE 94411/94627 show a large range in refractory lithophile element abundances (from ~5–6× CI to <0.01× CI), which correlate with textural type and size of chondrules: large, barred-olivine chondrules are enriched in refractory lithophile elements compared to small, cryptocrystalline chondrules (Russell *et al.*, 2000b; Krot *et al.*, 2001). These observations were interpreted as a result of fractional condensation either of chondrules or chondrule precursors in a closed system (Russell *et al.*, 2000b; Krot *et al.*, 2001). According to this model, barred-olivine chondrules formed first and were subsequently isolated from the nebular gas either by physical removal from the chondrule-forming region or by coarsening of fine-grained precursors during chondrule formation; cryptocrystalline chondrules formed later from a gas depleted in refractory lithophile elements (Krot *et al.*, 2001). The observed positive correlation between chondrule size and refractory lithophile element abundances is inconsistent with the origin of Al-rich chondrules by partial evaporation of ferromagnesian chondrule precursors (MacPherson and Huss, 2000).

The Al-diopside-rich chondrules are compositionally and mineralogically rather similar to the Al-rich barred-olivine chondrules; the former, however, are slightly depleted in Cr (Table 8; Figs. 8a,b and 14). This suggests that Al-diopside-rich chondrules could be genetically related to barred-olivine chondrules; both chondrule types may have formed in the same event. The observed enrichment in Al, Ca, and Ti, and depletion in Cr of Al-diopside-rich chondrules compared to barred-olivine chondrules may indicate that the Al-diopside-rich chondrules were isolated from the nebular gas at higher ambient temperatures than barred-olivine chondrules. Yet, the observed similarity in O-isotopic compositions of the Al-diopside-rich chondrules and the even more refractory CAIs in HH 237 and QUE 94411/94627 suggests that these components formed from an isotopically similar reservoir. Perhaps, CAIs, Al-diopside-rich chondrules, and barred-olivine chondrules formed at high temperatures in the closed system. An oxygen isotopic study of barred-olivine chondrules in QUE 94411/94627 and HH 237 may help to resolve this issue.

Acknowledgements–We thank the Meteorite Working Group, the Smithsonian Institution, the American Museum of Natural History, New York, and the Max-Planck-Institut für Chemie, Mainz, for the loan of polished sections of Hammadah al Hamra 237, QUE 94411, and QUE 94626. We are grateful to H. C. Connolly and A. Bischoff for constructive reviews. We also thank associate editor I. Lyon for useful comments and suggestions. This work was supported by NASA grants NAG 5-4212 (K. Keil, P. I.) and NAG 5-10610 (A. N. Krot, P. I.). This is Hawaii Institute of Geophysics and Planetology Publication No. 1167 and School of Ocean and Earth Science and Technology Publication No. 5826.

Editorial handling: I. C. Lyon

REFERENCES

BECKETT J. R. AND STOLPER E. (1994) The stability of hibonite, melilite and other aluminous phases in silicate melts: Implications for the origin of hibonite-bearing inclusions from carbonaceous chondrites. *Meteoritics* **29**, 41–65.

BISCHOFF A. AND KEIL K. (1984) Al-rich objects in ordinary chondrites: Related origin of carbonaceous and ordinary chondrites and their constituents. *Geochim. Cosmochim. Acta* **48**, 693–709.

BISCHOFF A., KEIL K. AND STÖFFLER D. (1985) Perovskite-hibonite-spinel-bearing inclusions and Al-rich chondrules and fragments in enstatite chondrites. *Chem. Erde* **44**, 97–106.

BISCHOFF A. *ET AL.* (1993a) Paired Renazzo-type (CR) carbonaceous chondrites from the Sahara. *Geochim. Cosmochim. Acta* **57**, 1587–1603.

BISCHOFF A., PALME H., SCHULTZ L., WEBER D., WEBER H. AND SPETTEL B. (1993b) Acfer 182 and paired samples, an iron-rich carbonaceous chondrite: Similarities with ALH85085 and relationship to CR chondrites. *Geochim. Cosmochim. Acta* **57**, 2631–2648.

BLANDER M. AND FUCHS L. H. (1975) Calcium-aluminum-rich inclusions in the Allende meteorite: Evidence for a liquid origin. *Geochim. Cosmochim. Acta* **39**, 1605–1619.

CAMPBELL A. J., HUMAYUN M., MEIBOM A., KROT A. N. AND KEIL K. (2001) Origin of metal grains in the QUE94411 chondrite. *Geochim. Cosmochim. Acta* **65,** 163–180.

CHIZMADIA L. J. AND RUBIN A. E. (2000) Petrology and origin of amoeboid olivine inclusions in CO3 chondrites (abstract). *Lunar Planet. Sci.* **31**, #1494, Lunar and Planetary Institute, Houston, Texas, USA (CD-ROM).

CLAYTON R. N., GROSSMAN L. AND MAYEDA T. K. (1973) A component of primitive nuclear composition in carbonaceous meteorites. *Science* **182**, 485–488.

CLAYTON R. N., ONUMA N., GROSSMAN L. AND MAYEDA T. K. (1977) Distribution of the pre-solar components in Allende and other carbonaceous chondrites. *Earth Planet. Sci. Lett.* **34**, 209–224.

CLAYTON R. N., MACPHERSON G. J., HUTCHEON I. D., DAVIS A. M., GROSSMAN L., MAYEDA T. K., MOLINI-VELSKO C. AND ALLEN J. M. (1984) Two forsterite-bearing FUN inclusions in the Allende meteorite. *Geochim. Cosmochim. Acta* **48**, 535–549.

DAVIS A. M., MACPHERSON G. J., CLAYTON R. N., MAYEDA T. K., SYLVESTER P. J., GROSSMAN L., HINTON R. W. AND LAUGHLIN J. R. (1991) Melt solidification and late stage evaporation of a FUN inclusion from the Vigarano C3V chondrite. *Geochim. Cosmochim. Acta* **55**, 621–638.

DAVIS A. M., MCKEEGAN K. D. AND MACPHERSON G. J. (2000) Oxygen-isotopic compositions of individual minerals from the FUN inclusion Vigarano 1623-5 (abstract). *Meteorit. Planet. Sci.* **35 (Suppl.)**, A47.

DOMINIK B., JESSBERGER E. K., STAUDACHER TH., NAGEL K. AND EL GORESY A. (1978) A new type of white inclusion in Allende: Petrography, mineral chemistry, $^{40}Ar/^{39}Ar$ ages, and genetic implications. *Proc. Lunar Planet. Sci. Conf.* **9th**, 1249–1266.

ENDREβ M., KEIL K., BISCHOFF A., SPETTEL B., CLAYTON R. N. AND MAYEDA T. K. (1994) Origin of dark clasts in the Acfer 059/El Djouf 001 CR2 chondrite. *Meteoritics* **29**, 26–40.

FAGAN T. J., KROT A. N. AND KEIL K. (2000) Calcium-aluminum-rich inclusions in enstatite chondrites (I): Mineralogy and textures. *Meteorit. Planet. Sci.* **35,** 771–783.

GREENWOOD R. C., HUTCHISON R., HUSS G. R. AND HUTCHEON I. D. (1992) CAIs in CO3 chondrites: Parent body or nebular alteration? (abstract). *Meteoritics* **27**, 229.

GREENWOOD R. C., LEE M. R., HUTCHISON R. AND BARBER D. J. (1994) Formation and alteration of CAIs in Cold Bokkeveld (CM2). *Geochim. Cosmochim. Acta* **58**, 1913–1935.

GRESHAKE A. J., KROT A. N., MEIBOM A. AND KEIL K. (2000) Transmission electron microscope study of CI-like matrix lumps in CH- and Bencubbin/CH-like chondrites (abstract). *Meteorit. Planet. Sci.* **35 (Suppl.)**, A47.

GROSSMAN L. (1980) Refractory inclusions in the Allende meteorite. *Ann. Rev. Earth Planet. Sci.* **8**, 559–608.

GROSSMAN J. N., RUBIN A. E. AND MACPHERSON G. J. (1988) ALH 85085: A unique volatile-poor carbonaceous chondrite with possible implications for nebula fractionation processes. *Earth Planet. Sci. Lett.* **91**, 33–54.

GUAN Y., MCKEEGAN K. D. AND MACPHERSON G. J. (1999) Calcium-aluminum-rich inclusions in unequilibrated enstatite chondrites: A preliminary petrologic and isotopic study (abstract). *Lunar Planet. Sci.* **31**, #1744, Lunar and Planetary Institute, Houston, Texas, USA (CD-ROM).

HASHIMOTO A. AND GROSSMAN L. (1987) Alteration of Al-rich inclusions inside amoeboid olivine aggregates in the Allende meteorite. *Geochim. Cosmochim. Acta* **51**, 1685–1704.

HERZOG G. F., FLYNN G. J., SUTTON S. R., DELANEY J. S., KROT A. N. AND MEIBOM A. (2000) Low gallium and germanium contents in metal grains from the Bencubbin/CH-like meteorite QUE 94411 determined by synchrotron XRF (abstract). *Meteorit. Planet. Sci.* **35 (Suppl.)**, A71.

KALLEMEYN G. W., RUBIN A. E. AND WASSON J. T. (1991) The compositional classification of chondrites. 5. The Karoonda (CK) group of carbonaceous chondrites. *Geochim. Cosmochim. Acta* **55**, 881–892.

KALLEMEYN G. W., RUBIN A. E. AND WASSON J. T. (1994) The compositional classification of chondrites: 6. The CR carbonaceous chondrite group. *Geochim. Cosmochim. Acta* **58**, 2873–2888.

KELLER L. P., CLARK J. C., LEWIS C. F. AND MOORE C. B. (1992) Maralinga, a metamorphosed carbonaceous chondrite found in Australia. *Meteoritics* **27**, 87–91.

KIMURA M., EL GORESY A., PALME H. AND ZINNER E. (1993) Ca-, Al-rich inclusions in the unique chondrite ALH85085: Petrology, chemistry, and isotopic compositions. *Geochim. Cosmochim. Acta* **57**, 2329–2359.

KOMATSU M., KROT A. N., PETAEV M. I., ULYANOV A. A., KEIL K. AND MIYAMOTO M. (2001) Mineralogy and petrography of amoeboid olivine aggregates from the reduced CV3 chondrites Efremovka, Leoville and Vigarano: Products of nebular condensation, accretion, and annealing. *Meteorit. Planet. Sci.* **36**, 629–641.

KROT A. N. (2000) Anorthite-rich chondrules from primitive carbonaceous chondrites: Genetic links between CAI and chondrules (abstract). *Meteorit. Planet. Sci.* **35 (Suppl.)**, A93.

KROT A. N., ULYANOV A. A. AND WEBER D. (1999) Al-diopside-rich refractory inclusions in the CH chondrite Acfer 182 (abstract). *Lunar Planet. Sci.* **30**, #2018, Lunar and Planetary Institute, Houston, Texas, USA (CD-ROM).

KROT A. N., MCKEEGAN K. D., ZIPFEL J., WEISBERG M. K., MEIBOM A., RUSSELL S. S. AND KEIL K. (2000a) Refractory inclusions and Al-rich chondrules in Bencubbin/CH-like carbonaceous chondrites Hammadah al Hamra 237 and QUE 94411 (abstract). *Lunar Planet. Sci.* **31,** #1448, Lunar and Planetary Institute, Houston, Texas, USA (CD-ROM).

KROT A. N., ULYANOV A. A. AND KEIL K. (2000b) Forsterite-bearing Ca, Al-rich inclusion from the reduced CV chondrite Efremovka (abstract). *Meteorit. Planet. Sci.* **35 (Suppl.)**, A93–A94.

KROT A. N., MEIBOM A., RUSSELL S. S., ALEXANDER C. M. O'D., JEFFRIES T. E. AND KEIL K. (2001) A new astrophysical setting for chondrule formation. *Science* **291**, 1776–1779.

MACPHERSON G. J. AND DELANEY J. S. (1985) A fassaite-two olivine-pleonaste-bearing refractory inclusion from Karoonda (abstract). *Lunar Planet. Sci.* **16**, 515–516.

MACPHERSON G. J. AND HUSS G. (2000) Convergent evolution of CAIs and chondrules: Evidence from bulk compositions and a cosmochemical phase diagram (abstract). *Lunar Planet. Sci.* **31**, #1796, Lunar and Planetary Institute, Houston, Texas, USA (CD-ROM).

MACPHERSON G. J., BAR-MATTHEWS M., TANAKA T., OLSEN E. AND GROSSMAN L. (1983) Refractory inclusions in the Murchison meteorite. *Geochim. Cosmochim. Acta* **47**, 823–839.

MACPHERSON G. J., GROSSMAN L., HASHIMOTO A., BAR-MATTHEWS M. AND TANAKA T. (1984) Petrographic studies of refractory inclusions from the Murchison meteorite. *Proc. Lunar Planet. Sci. Conf.* **15th**, *J. Geophys. Res. Suppl.* **89**, C299–C312.

MACPHERSON G. J., WARK D. A. AND ARMSTRONG J. T. (1988) Primitive material surviving in chondrites: Refractory inclusions. In *Meteorites and the Early Solar System* (eds. J. F. Kerridge and M. S. Matthews), pp. 746–807. Univ. Arizona Press, Tucson, Arizona, USA.

MACPHERSON G. J., DAVIS A. M. AND GROSSMAN J. N. (1989) Refractory inclusions in the unique chondrite ALH 85085 (abstract). *Meteoritics* **23**, 143.

MCKEEGAN K. D., LESHIN L. A., RUSSELL S. S. AND MACPHERSON G. J. (1997) Ion microprobe measurements reveal large oxygen-16 excesses in calcium-aluminum-rich inclusions of an ordinary chondrite (abstract). *Meteorit. Planet. Sci.* **32 (Suppl.)**, A88–A89.

MCKEEGAN K. D., LESHIN L. A., RUSSELL S. S. AND MACPHERSON G. J. (1998a) Oxygen isotope abundances in calcium-aluminum-rich inclusions from ordinary chondrites; Implications for nebular heterogeneity. *Science* **280,** 414–418.

MCKEEGAN K. D., LESHIN L. A. AND MACPHERSON G. J. (1998b) Oxygen-isotopic stratigraphy in a Vigarano type A calcium-aluminum-rich inclusion (abstract). *Meteorit. Planet. Sci.* **33 (Suppl.)**, A102–A103.

MCSWEEN H.Y., JR. (1977) Chemical and petrographic constraints on the origin of chondrules and inclusions in carbonaceous chondrites. *Geochim. Cosmochim. Acta* **41**, 1843–1860.

MEIBOM A., DESCH S. J., PETAEV M. I., KROT A. N., CUZZI J. N., WOOD J. A. AND KEIL K. (2000) An astrophysical model for the formation of zoned Fe,Ni metal grains in the Bencubbin/CH-like chondrites QUE 94411 and Hammadah al Hamra 237 (abstract). *Meteorit. Planet. Sci.* **35 (Suppl.)**, A107.

NOGUCHI T. (1993) Petrology and mineralogy of CK chondrites: Implications for the metamorphism of the CK chondrite parent body. *Proc. NIPR Symp. Antarct. Meteorites* **6**, 204–233.

PETAEV M. I., MEIBOM A., KROT A. N., WOOD J. A. AND KEIL K. (2001) The condensation origin of zoned grains in Queen Alexandra Range 94411: Implications for the formation of the Bencubbin-like chondrites. *Meteorit. Planet. Sci.* **36**, 93–106.

RUSSELL S. S., HUSS G. R., FAHEY A. J., GREENWOOD R. C., HUTCHISON R. AND WASSERBURG G. J. (1998) An isotopic and petrologic study of calcium-aluminum-rich inclusions from CO3 meteorites. *Geochim. Cosmochim. Acta* **62**, 689–714.

RUSSELL S. S., DAVIS A. M., MACPHERSON G. J., GUAN Y. AND HUSS G. J. (2000a) Refractory inclusions from the ungrouped carbonaceous chondrites MacAlpine Hills 87300 and 88107. *Meteorit. Planet. Sci.* **35**, 1051–1067.

RUSSELL S. S., KROT A. N., MEIBOM A., ALEXANDER C. M. O'D. AND JEFFRIES T. E. (2000b) Chondrules of the first generation? Trace-element geochemistry of silicates from Bencubbin/CH-like meteorites (abstract). *Meteorit. Planet. Sci.* **35 (Suppl.)**, A139.

SCOTT E. R. D. (1988) A new kind of primitive chondrite, Allan Hills 85085. *Earth Planet. Sci. Lett.* **91**, 1–18.

SIMON S. B., YONEDA S., GROSSMAN L. AND DAVIS A. M. (1994) A $CaAl_4O_7$-bearing refractory spherule from Murchison: Evidence for very high-temperature melting in the solar nebula. *Geochim. Cosmochim. Acta* **58**, 1937–1949.

SIMON S. B., MCKEEGAN K. D., EBEL D. S. AND GROSSMAN L. (2000) Complexely zoned Cr-Al spinel found *in situ* in the Allende meteorite. *Meteorit. Planet. Sci.* **35**, 215–228.

STOLPER E. (1982) Crystallization sequences of Ca-Al-rich inclusions from Allende: An experimental study. *Geochim. Cosmochim. Acta* **46**, 2159–2180.

WARK D. A., BOYNTON W. V., KEAYS R. R. AND PALME H. (1987) Trace element and petrologic clues to the formation of forsterite-bearing Ca-Al-rich inclusions in the Allende meteorite. *Geochim. Cosmochim. Acta* **51**, 607–622.

WASSON J. T. AND KALLEMEYN G. W. (1990) Allan Hills 85085: A subchondritic meteorite of mixed nebular and regolithic heritage. *Earth Planet. Sci. Lett.* **101**, 148–161.

WEBER D. AND BISCHOFF A. (1992) Ca-dialuminate ($CaAl_4O_7$)—A dominating phase in Ca,Al-rich inclusions from Acfer-182 (abstract). *Meteoritics* **27**, 304–305.

WEBER D. AND BISCHOFF A. (1994) The occurrence of grossite ($CaAl_4O_7$) in chondrites. *Geochim. Cosmochim. Acta* **18**, 3855–3877.

WEBER D. AND BISCHOFF A. (1997) Refractory inclusions in the CR chondrite Acfer 059–El Djouf 001: Petrology, chemical composition, and relationship to inclusion populations in other types of carbonaceous chondrites. *Chem. Erde* **57**, 1–24.

WEBER D., ZINNER E. AND BISCHOFF A. (1995) Trace element abundances and magnesium, calcium, and titanium isotopic compositions of grossite-containing inclusions from the carbonaceous chondrite Acfer 182. *Geochim. Cosmochim. Acta* **59**, 803–823.

WEISBERG M. K. AND PRINZ M. (1990) Refractory inclusions in CR2 (Renazzo-type) chondrites (abstract). *Lunar Planet. Sci.* **21**, 1315–1316.

WEISBERG M. K., PRINZ M., CLAYTON R. N. AND MAYEDA T. K. (1993) The CR (Renazzo-type) carbonaceous chondrite group and its implications. *Geochim. Cosmochim. Acta* **57**, 1567–1586.

WEISBERG M. K., PRINZ M., CLAYTON R. N., MAYEDA T. K., SUGIURA N. AND ZASHU S. (1998) The bencubbinite (B) group of the CR clan (abstract). *Meteorit. Planet. Sci.* **33 (Suppl.)**, A166.

WEISBERG M. K., PRINZ M., CLAYTON R. N., MAYEDA T. K., SUGIURA N., ZASHU S. AND EBIHARA M. (2001) A new metal-rich chondrite grouplet. *Meteorit. Planet. Sci.* **36**, 401–418.

ZIPFEL J., WLOTZKA F. AND SPETTEL B. (1998) Bulk chemistry and mineralogy of a new "unique" metal-rich chondritic breccia, Hammadah al Hamra 237 (abstract). *Lunar Planet. Sci.* **29**, #1417, Lunar and Planetary Institute, Houston, Texas, USA (CD-ROM).